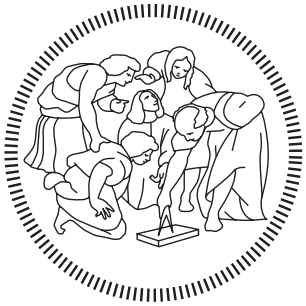

POLITECNICO
MILANO 1863

School of Industrial and Information Engineering

Master of Science in Space Engineering

Characterization of the tropospheric attenuation affecting Earth-space links using ERA5 data

Supervisor: Prof. Lorenzo Luini

Author: Estelle Pelat

ID number: 916010

Academic Year 2019/2020

ACKNOWLEDGEMENTS

I would like to thank all the people who helped me to go through this thesis and supported me during these two years at Politecnico di Milano. First, I wish to express profuse thanks to Professor Luini, supervisor of this thesis. He made himself extremely available to answer all my questions and to help me. Even in this particular pandemic context, where I had to work from home in France, far from Milan, Professor Luini provided me with careful support and useful advice. I would like also to thank my boyfriend, Thomas, who helped me a lot with this thesis. I am grateful to him for his Matlab advice, and for the countless times he managed to find errors in my codes.

I also would like to thank my home university, Supméca. They offered me the incredible chance to do a double degree at Politecnico di Milano, in Space Engineering, my dream master. I am really grateful to them to have provided me with a strong practical background, and to Politecnico di Milano for the theoretical knowledge. Finally, I would like to thank my family and my friends, who supported me and encouraged me throughout this thesis, and more in general throughout these two years.

CONTENTS

LIST OF FIGURES

LIST OF TABLES

ABSTRACT

In this work, the main tropospheric impairments on an Earth-space link are investigated using the ERA5 dataset. Indeed, when an electromagnetic wave crosses the troposphere, it has to face clouds, rain and gases that cause signal attenuation. These three types of attenuation are studied using the latest climate reanalysis produced by the European Centre for Medium-Range Weather Forecast in 2020, ERA5, providing hourly data on many atmospheric, land-surface and sea-state parameters. ERA5 has a number of innovative features. These include a significantly enhanced horizontal resolution, hourly output throughout and an uncertainty estimate .Therefore, the objective of this work is to assess if and to what extent the ERA5 data can be used to estimate directly the tropospheric attenuation, not withstanding their limited spatial and temporal resolutions. To this aim, the Earth-space link between the Alphasat satellite, a large geostationary communications satellite, and a ground station in Milan (Italy) is studied at two downlink beacons frequencies: 19.7 GHz and 39.4 GHz. The data of interest from the ERA5 dataset were dowloaded for the entire year of 2018. Clouds, rain and gaseous attenuations are calculated over the year using the ITU-R Recommendations. The total attenuation is also computed, as well as the complementary cumulative distribution functions for each dissipative constituent.

1 INTRODUCTION

1.1 Context of investigation

In 1957, Sputnik 1, the first artificial Earth satellite was launched in orbit around the Earth (Terry, 2013). This was a major breakthrough in the spatial conquest. From this moment, more and more satellites were sent into orbit. Recently, their applications are expanding to areas such as, remote sensing, military surveillance, science missions, and communications. But all these systems have to face the same issue: signal attenuation due to wave propagation. The amplitude of the received signal can be reduced from the free space value (Ippolito, 1989), and it has to be taken into account during the satellite design. Indeed, an important part of satellite design is the link budget calculation. To compute the power received at the antenna in a medium like the atmosphere, the attenuation induced by this medium is needed. Moreover, it can be useful to exploit past atmospheric attenuation data to predict the future one. This way, space systems and operations can be adapted to the incoming situations.

1.2 Troposphere and attenuation

In the context of Earth-space communication systems, where guided propagation is no longer applicable, it is necessary to transmit information by means of the propagation of electromagnetic waves. They cross the terrestrial atmosphere which strongly affects the wave propagation. The atmosphere is made of two main regions: the troposphere and the ionosphere. The troposphere refers to the lowest layers of the atmosphere where meteorological phenomena take place (Danielson, Levin, & Abrams, 2002). In general, the impact of the troposphere tends to increase with the wave frequency. The ionosphere concerns the upper layers of the atmosphere, where the components are partially ionized by solar radiations. These ionisations also have an impact on the wave propagation. Contrary to the troposphere, these effects dominate at low frequencies, below 1 GHz, and decrease with the increase in the frequency.

The troposphere is the atmosphere region that extends from the ground up to 20 km, depending on the location and the season. Composed by a mixture of different gases (78.08% nitrogen, 20.95% oxygen, 0.93% argon, 0.04% carbon dioxide, and small amount of other gases), it contains 75% of the atmosphere's mass and 99% of the total mass of water vapour and aerosols (McGraw-Hill, 2009). Dry air, whose density exponentially decreases with altitude, and water vapour, whose quantity is variable, give to this medium a refractive index slightly higher than 1, causing absorption depending on meteorological conditions. For frequencies between 1 and 1000 GHz, the effects on the wave propagation induced by the troposphere can be classified in 3 categories: attenuation, scintillation, and depolarisation.

The attenuation consists of a signal loss because of an absorption phenomenon due to the presence of gaseous particles or hydrometeors along the link. Between 1 and 1000 GHz, the gaseous components are mainly dry air and water vapour. The hydrometeors are mainly clouds, rain and snow (Castanet & Lassudrie-Duchesne, 2008).

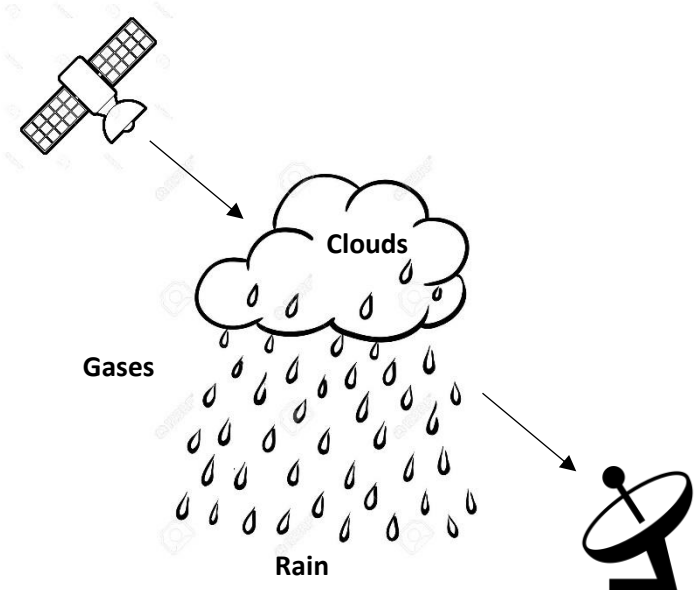

Figure 1: Cloud, rain and gaseous attenuations along an Earth-space link

1.3 ERA5 reanalysis

To compute the tropospheric attenuation, the ERA5 reanalysis dataset was used. A reanalysis is a scientific method to develop a comprehensive record of how weather and climate are changing over time by combining short-range forecast data with observations to produce the best fit to both. ERA5 is the very last dataset available from the ECMWF. It is the fifth generation of ECMWF atmospheric reanalysis of the global climate, which started with the FGGE reanalysis produced in the 1980s, following by ERA-15, ERA-40, ERA-Interim and finally ERA5 (ERA5 - Forecast - Dataset, 2020).

The ERA5 dataset innovates in many ways. It has a higher resolution than ERA-Interim. Indeed, the ERA5 atmospheric data has a spatial resolution of 31km, 0.28125°. The vertical direction is divided in 137 model levels, with the top level at 0.01 hPa. Atmospheric data are available on these levels and they are also interpolated to 37 pressure, 16 potential temperature and 1 potential vorticity level(s). Surface or single level data are also available. The ERA5 dataset cover the period from January 1950 on an hourly basis. The resolution of ERA5 data is summarized in Table 1.

Table 1: ERA5 dataset resolution

ERA 5 RESOLUTION	
Horizontal resolution	31 km, 0.28125° on Gaussian grid
Vertical resolution	137 model levels 37 pressure levels 16 potential temperature levels 1 potential vorticity level 1 surface level
Temporal resolution	1 hour

2 INPUT DATA

2.1 Ground station and satellite

This thesis focuses on a specific ground station/satellite duo. The satellite is Alphasat, launched on July 25, 2013, from the European Spaceport in Kourou, French Guiana. It is a large geostationary communications satellite, providing mobile communications to Africa and parts of Europe and Asia (Rossi, et al., 2016). The gound station is located in Milan, Italy. The detailed positions of the satellite and ground station can be found in the following tables:

Table 2: Alphasat coordinates

ALPHASAT	
Latitude	0°
Longitude	25°E
Orbital plane inclinaison	0°+3°

Table 3: Ground station coordinates

GROUND STATION	
Latitude	45.47867°N
Longitude	9.232760°E
Altitude	0.138 km a.m.s.l

Table 4: Link coordinates

LINK	
Elevation (average)	35.42°
Azimuth (average)	158.38°

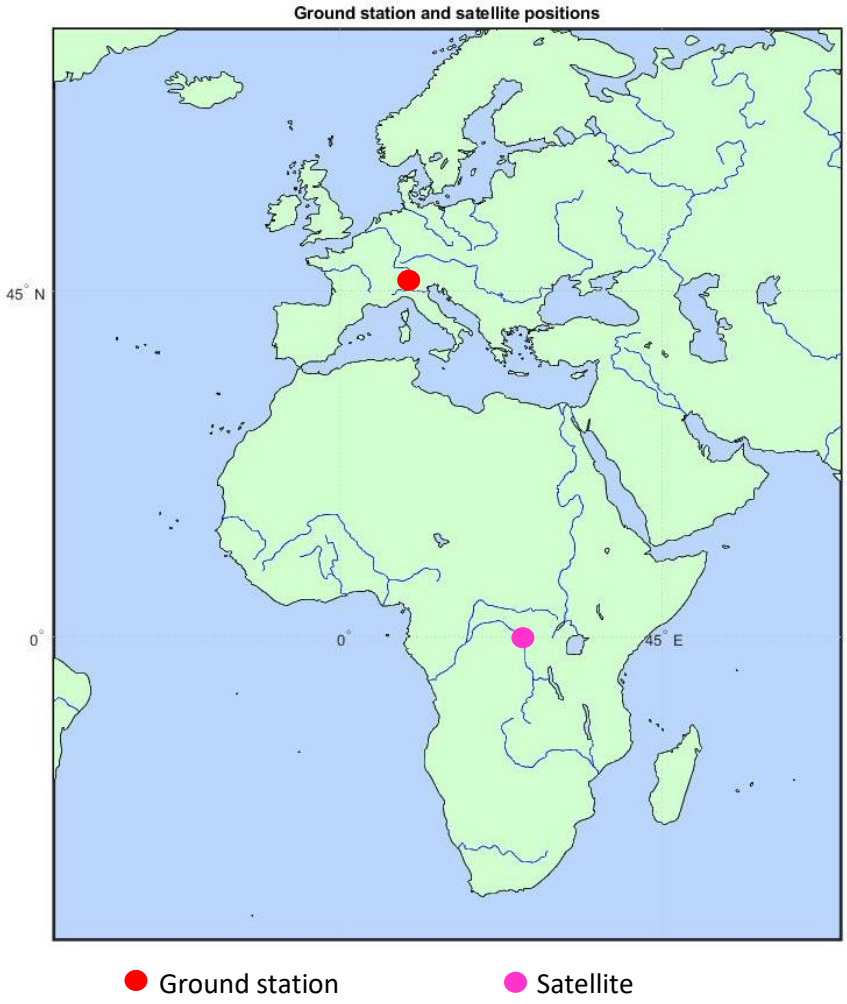

Figure 2: Ground station and satellite position

2.2 Frequency of study

Most satellite communication systems operate at frequencies in the range of 2-18 GHz (S, C, X and Ku bands). However such frequency bands have a limited bandwidth which results today in their saturation. Indeed, with the exponential development of multimedia services (internet, video, data transfer, etc.), the low frequency bands are congested (Rossi, et al., 2016). Such demands impose as a consequence to reach frequency bands higher than 20 GHz: Ka band (26.5-40 GHz) and W band (75-110 GHz) for civil telecommunications and, more in general, EHF (Extremely High Frequencies) band for military telecommunications. But operating at high frequency raises a problem: atmospheric impairments on the electromagnetic wave propagation. In fact, the higher the frequency, the greater the attenuation affecting the signal. Using satellite beacon

signal as a reference signal in satellite wave propagation study, is one of the most important methods to study the effects of the atmosphere. Satellite beacons are frequently available for pointing large antennas, but such signals can also be used for measuring the effect of natural phenomena such as atmospheric gases, water vapour, oxygen molecules, clouds, rain, dust and fog, existing in different layers of the atmosphere, including troposphere and ionosphere (Bahri, Yarmohammadi, Keshavarzi, & Moradi, 2015). This thesis will focus on two downlink beacons: the Ka-band beacon, at 19.7 GHz, and the Q-band beacon at 39.4 GHz (Rossi, et al., 2016).

2.3 Area of study

In order to retrieve the ERA5 dataset, an area of study needs to be determined. The needed area is computed from the position of the ground station, the link elevation and the height of the troposphere. Setting the troposphere height at 20 km, and assuming the Earth to be a perfect sphere, the area is calculated. Figure 3 shows this area in red:

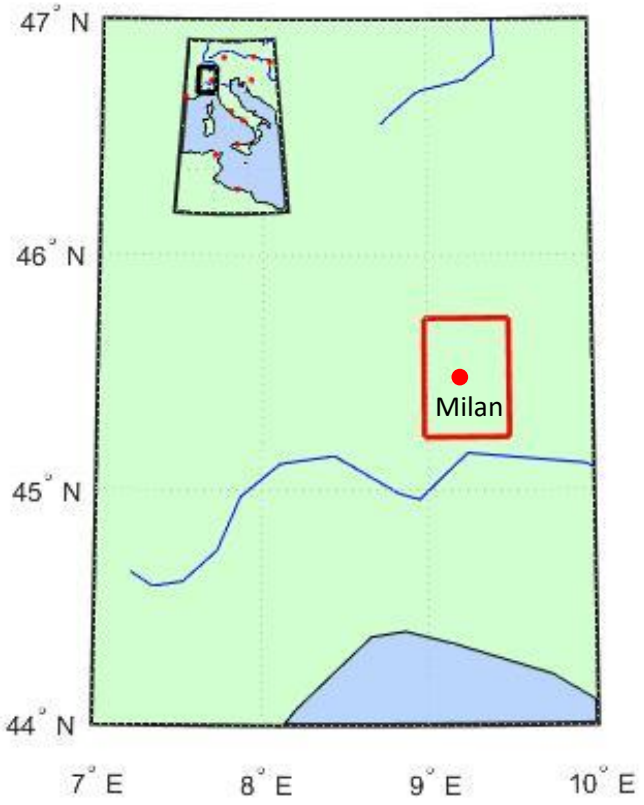

Figure 3: Area of study

The area coordinates are:

North: 45.7316°N West: 8.9813°E South: 45.2258°N East: 9.4960°E

Which corresponds to an area of 57.232 km × 56.244 km.

After setting the area of study in order to download the corresponding data, the path of the signal, given in latitude/longitude/altitude, must be identified. To this aim, the path is discretized as shown in Figure 4 .

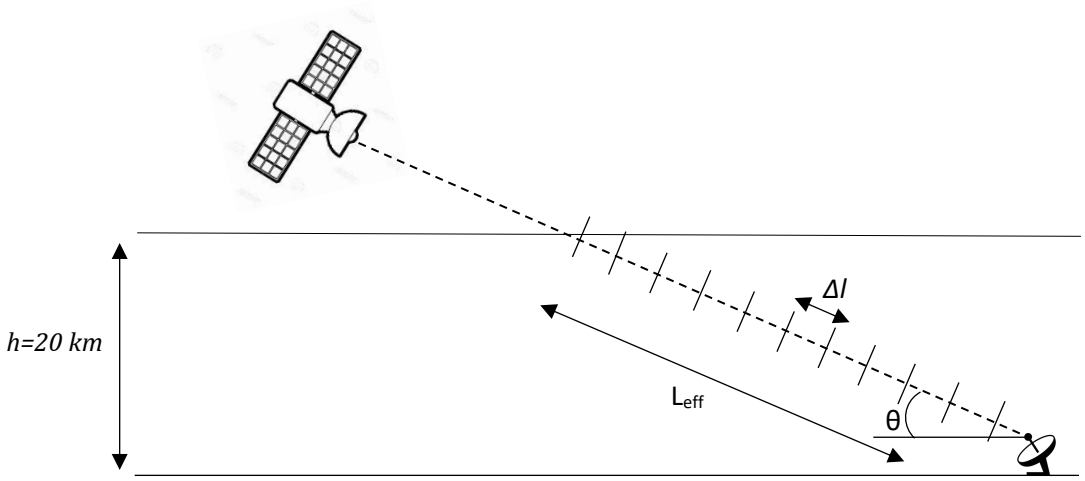

Figure 4: Discretization of the path

Knowing the elevation angle θ and the troposphere height h, the effective length of the path crossing the troposphere can be computed as:

$$L_{eff} = \frac{h}{\sin(\theta)} \tag{2.3.1}$$

The path can be discretized in n points distant of $\Delta l=1km$, each of them having one longitude, one latitude and one altitude. Then, the longitude and latitude giving by ERA5 that are the closest to the discretized points have to be found. Since the ERA5 data have a smaller resolution than the discretized path, several points will have the same longitude and latitude. This give three pixels crossed by the link. Figure 5 shows a projection of the link on the ground (in red) crossing the three pixels.

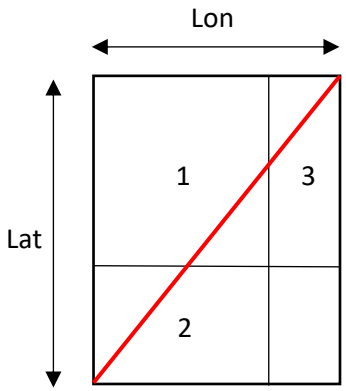

Figure 5: Pixels crossed by the link

Where the three pixels have the following coordinates:

Pixel n°1: Longitude = 9.2813°E ; Latitude = 45.3258°N
Pixel n°2: Longitude = 9.2813°E ; Latitude = 45.4258°N
Pixel n°3: Longitude = 9.3813°E ; Latitude = 45.3258°N

2.4 Downloaded data

As introduced in section 1.3, the ERA5 dataset was used in this thesis. The data were retrieved for the entire year of 2018, for the area specified in section 2.3. All the needed parameters were downloaded in netCDF format specifying a regular spatial grid of 0.1°/0.1°. As listed in Table 1, the ERA5 dataset spatial resolution is 0.28125°, which is smaller than the grid specified for the download. A higher output resolution than the archived resolution can be specified, but the resulting data will not contain any more information than the original, it has merely been interpolated to a higher resolution. This makes the output look smoother, but does not increase the accuracy or precision of the data. All the data were retrieved in model levels, except for the *Total Column Rain Water*, which was retrieved as surface data.

The following data have been downloaded:

- *Longitude*: according to the spatial resolution of the ERA5 dataset, and the area of study specified, a list of the relevant longitudes was retrieved.
  Lon= [8.9813; 9.0813; 9.1813; 9.2813; 9.3813; 9.4813]
- *Latitude*: same as longitude, a list of the relevant latitudes was retrieved.

Lat= [45.7258; 45.6258; 45.5258; 45.4258; 45.3258]

- *Levels*: according to the vertical resolution of the ERA5 dataset in model levels, a list of 137 levels was retrieved.
- *Time*: ERA5 data are retrieved on an hourly basis, giving a time list, which has as unit 'hours since 01-01-1900'.
- *Temperature*: Air temperature, in K, size [lon*lat*levels*time].
- *Specific rain water content*: in kg/kg, the mass of water reduced from large-scale clouds that is of raindrop size and so can fall to the surface as precipitation, size [lon*lat*levels*time].
- *Specific cloud liquid water content*: in kg/kg, the mass of cloud liquid water droplets per kilogram of the total mass of moist air, size [lon*lat*levels*time].
- *Specific humidity*: in kg/kg, the mass of water vapour per kilogram of moist air, size [lon*lat*levels*time].
- *Total column rain water*: in (kg/m^2) equivalent to mm, this parameter is the total amount of water in droplets of raindrop size which can fall on the surface as precipitation in a column extending from the surface of the Earth to the top of the atmosphere, size [lon*lat*time].

The *density* (kg/m^3), *altitude* (m) and *pressure* (Pa) corresponding to each level were retrieved thanks to the L137 model level definitions. They are based on the 1976 version of the International Civil Aviation Organization Standard Atmosphere (Administration, 1976).

3 ELECTROMAGNETIC WAVE PROPAGATION THROUGH TROPOSPHERE

When an electromagnetic wave is travelling through the atmosphere, like in the case of an Earth-Space communication link, the wave has to face several propagation impairments. In the troposphere, which is the region where meteorological phenomena take place, electromagnetic waves encounter gases and hydrometeors, which results in signal depolarization and attenuation. Other tropospheric effects exist, just as refraction due to the spatial inhomogeneities in the atmosphere layers, but this thesis will focus on the tropospheric attenuation.

3.1 Physical concepts

The very first step when dealing with electromagnetic wave propagation is the Maxwell's equations, governing the EM wave propagation in a medium:

$$\overrightarrow{rot}\,\vec{E} = -\mu\frac{d\vec{H}}{dt} \tag{3.1.1}$$

$$\overrightarrow{rot}\,\vec{H} = \varepsilon\frac{\overrightarrow{d\vec{E}}}{dt} + \vec{J} + \sigma\vec{E} \tag{3.1.2}$$

$$div\,\vec{E} = \frac{\rho}{\varepsilon} \tag{3.1.3}$$

$$div\,\vec{H} = 0 \tag{3.1.4}$$

where $\vec{E}$ is the electric field, $\vec{H}$ is the magnetic field, ε is the dielectric permittivity of the medium, μ is the magnetic permeability of the medium, ρ is the total electric charge density, σ is the electrical conductivity of the medium and $\vec{J}$ is the conduction current density.

The directional energy flux of an electromagnetic field (W/m^2) is represented by the Poynting vector:

$$\vec{S} = \vec{E} \times \vec{H} \tag{3.1.5}$$

This form of the Poynting vector represents the instantaneous power flow due to instantaneous electric and magnetic fields. However, considering a time-averaged Poynting vector, this last one can be written as:

$$\langle S \rangle = \frac{1}{2} Re\left(\vec{E} \times \overrightarrow{H^*}\right) \tag{3.1.6}$$

where $\overrightarrow{H^*}$ is the complex conjugate of $\vec{H}$.

When a wave impinges on a particle, two effects take place: a part of the incident energy is scattered in all directions and another part is absorbed by the particle and transformed into heat by the Joule effect. As a result, both effects contributes to decreasing the power carried by the wave in the direction of the receiver. This is the attenuation phenomenon.

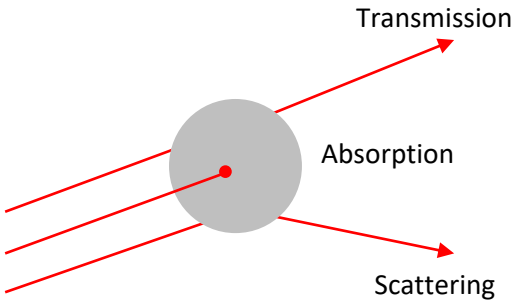

Figure 6: Attenuation phenomenon

Scattering takes place when a wave interacts with a body and its energy is absorbed and re-emitted in multiple directions with different intensities. More precisely, when a single electron, an atom, a molecule, or a solid of liquid particle is illuminated by an electromagnetic wave, electric charges in the obstacle are set into oscillatory motion by the electric field of the incident wave. Accelerated electric charges radiate electromagnetic energy in all directions: it is this secondary radiation that is called radiation scattered by the obstacle. In addition to reradiating electromagnetic energy, the excited elementary charges may transform part of the incident electromagnetic energy into other forms (thermal energy, for example), a process called absorption (Bohren & Huffman, 1998).

The power attenuation through a medium over a distance z can be written as (Shieh & Djordjevic, 2010):

$$\frac{dP}{dz} = -\alpha P \tag{3.1.7}$$

where α is the power attenuation per unit length. If P_0 is the power at $z_0 = 0$, then integrating between z_0 and z,

$$\ln \frac{P}{P_0} = -\int_{z_0}^{z} \alpha \, dz \tag{3.1.8}$$

The total relative power loss A (dB), also called attenuation, over a distance z, is given by:

$$A = 10 \, log \frac{P}{P_0} = \frac{10}{\ln 10} \ln \frac{P}{P_0} = -4.343 \int_{z_0}^{z} \alpha \, dz = -\int_{z_0}^{z} \gamma \, dz \tag{3.1.9}$$

where γ is the specific attenuation in dB/km.

As it can be seen in Figure 5, the signal between the satellite and the ground station is crossing several pixels. The contributions of these three pixels can be added in the following way:

$$A = -\left(\int_{z_0}^{z_1} \gamma_1 \, dz_1 + \int_{z_1}^{z_2} \gamma_2 \, dz_2 + \int_{z_2}^{z_3} \gamma_3 \, dz_3 \right) \tag{3.1.10}$$

3.2 Cloud attenuation theory

Clouds and fog are made of water drops in suspension whose size – generally less than 0.01 cm – can be considered as negligible for frequencies lower than 200 GHz (Srinivas & Ramana, 2017). In fact, the Rayleigh approximation can then be used to compute the cloud attenuation along slant paths with two parameters according to the recommendation ITU-R P.840-8 (ITU-R, 2019): the cloud liquid water specific attenuation coefficient K_l $(dB/km)/(g/m^3)$ and the liquid water density in the cloud or fog M (g/m^3).

The specific attenuation within a cloud or fog can be written as:

$$\gamma_{cloud}(f, T) = K_l(f, T) M \qquad (dB/km) \tag{3.2.1.1}$$

with K_l computed as following using a mathematical model based on Rayleigh scattering:

$$K_l(f, T) = \frac{0.819 f}{\varepsilon''(1+\eta^2)} \qquad (dB/km)/(g/m^3) \tag{3.2.1.2}$$

where f is the frequency (GHz) and:

$$\eta = \frac{2 + \varepsilon'}{\varepsilon''} \tag{3.2.1.3}$$

The complex dielectric permittivity of water is given by:

$$\varepsilon''(f) = \frac{f(\varepsilon_0 - \varepsilon_1)}{f_p\left[1+(f/f_p)^2\right]} + \frac{f(\varepsilon_1 - \varepsilon_2)}{f_s\left[1+(f/f_s)^2\right]} \quad (3.2.1.4)$$

$$\varepsilon'(f) = \frac{\varepsilon_0 - \varepsilon_1}{\left[1+(f/f_p)^2\right]} + \frac{\varepsilon_1 - \varepsilon_2}{\left[1+(f/f_s)^2\right]} + \varepsilon_2 \quad (3.2.1.5)$$

where:

$$\varepsilon_0 = 77.66 + 103.3(\theta - 1) \quad (3.2.1.6)$$

$$\varepsilon_1 = 0.0671\varepsilon_0 \quad (3.2.1.7)$$

$$\varepsilon_2 = 3.52 \quad (3.2.1.8)$$

$$\theta = 300/T \quad (3.2.1.9)$$

The principal relaxation frequency f_p, and secondary relaxation frequency f_s, are:

$$f_p = 20.20 - 146(\theta - 1) + 316(\theta - 1)^2 \qquad (GHz) \quad (3.2.1.10)$$

$$f_s = 39.8 f_p \qquad (GHz) \quad (3.2.1.11)$$

The liquid water density in the cloud M can be computed as following:

$$M = clwc \times 10^3 \rho \ \ (\mathrm{g/m^3}) \quad (3.2.1.12)$$

where *clwc* is the cloud liquid water content in kg/kg, ρ the density in ($\mathrm{kg/m^3}$).

Once γ_{cloud} is computed, the total rain attenuation along the path can be computed with:

$$A_{cloud} = \int_0^L \gamma_{cloud}(x)\, dx \quad (dB) \quad (3.2.1.13)$$

3.3 Rain attenuation theory

Rain attenuation is the major propagation impairment for satellite communications operating at the frequency above 10 GHz. Rain attenuation increases with the rain water content and can be computed with the rain rate (mm/hr). The presence of hydrometeors, particularly rain, in the propagation path causes scattering and absorption of the propagating wave. This is why the dropsize distribution of the water species must also enter the modelling of their interaction with an incoming plane wave.

3.3.1 Specific rain attenuation

The Recommendation ITU-R P.838-3 (ITU-R, Recommendation ITU-R P.838-3, Specific Attenuation Model for Rain for Use in Prediction Methods, 2005) allows to compute the specific rain attenuation thanks to a power law:

$$\gamma_{rain} = kR^{\alpha} \qquad (dB/km) \tag{3.3.1.1}$$

where R is the rain rate in mm/hr, k and α are coefficients depending on the frequency (from 1 to 1000 GHz) and on the polarization of the wave, and are given by the following equations:

$$\log_{10} k = \sum_{j=1}^{4} \left(a_j \exp\left[-\left(\frac{\log_{10} f - b_j}{c_j} \right)^2 \right] \right) + m_k \log_{10} f + c_k \tag{3.3.1.2}$$

$$\alpha = \sum_{j=1}^{5} \left(a_j \exp\left[-\left(\frac{\log_{10} f - b_j}{c_j} \right)^2 \right] \right) + m_\alpha \log_{10} f + c_\alpha \tag{3.3.1.3}$$

k and α can be either k^H *or* k^V, α^H or α^V, where H stands for horizontal and V for vertical polarization. Values for k^H are given in Table 5, for k^V in Table 6 for α^H in Table 7 and for α^V in Table 8.

Table 5: Coefficients for k^H

j	a_j	b_j	c_j	m_k	c_k
1	-5.3398	-0.10008	1.13098	-0.18961	0.71147
2	-0.35351	1.2697	0.454	-0.18961	0.71147
3	-0.23789	0.86036	0.15354	-0.18961	0.71147
4	-0.94158	0.64552	0.16817	-0.18961	0.71147

Table 6: Coefficients for k^V

j	a_j	b_j	c_j	m_k	c_k
1	-3.80595	0.56934	0.81061	-0.16398	0.63297
2	-3.44965	-0.22911	0.51059	-0.16398	0.63297
3	-0.39902	0.73042	0.11899	-0.16398	0.63297
4	0.50167	1.07319	0.27195	-0.16398	0.63297

Table 7: Coefficients for α^H

j	a_j	b_j	c_j	m_a	c_a
1	-0.14318	1.82442	-0.55187	0.67849	-1.95537
2	0.29591	0.77564	0.19822	0.67849	-1.95537
3	0.32177	0.63773	0.13164	0.67849	-1.95537
4	-5.3761	-0.9623	1.47828	0.67849	-1.95537
5	16.1721	-3.2998	3.4399	0.67849	-1.95537

Table 8: Coefficients for α^V

j	a_j	b_j	c_j	m_a	c_a
1	-0.07771	2.3384	-0.76284	-0.053739	0.83433
2	0.56727	0.95545	0.54039	-0.053739	0.83433
3	-0.20238	1.1452	0.26809	-0.053739	0.83433
4	-48.2991	0.791669	0.116226	-0.053739	0.83433
5	48.5833	0.791459	0.116479	-0.053739	0.83433

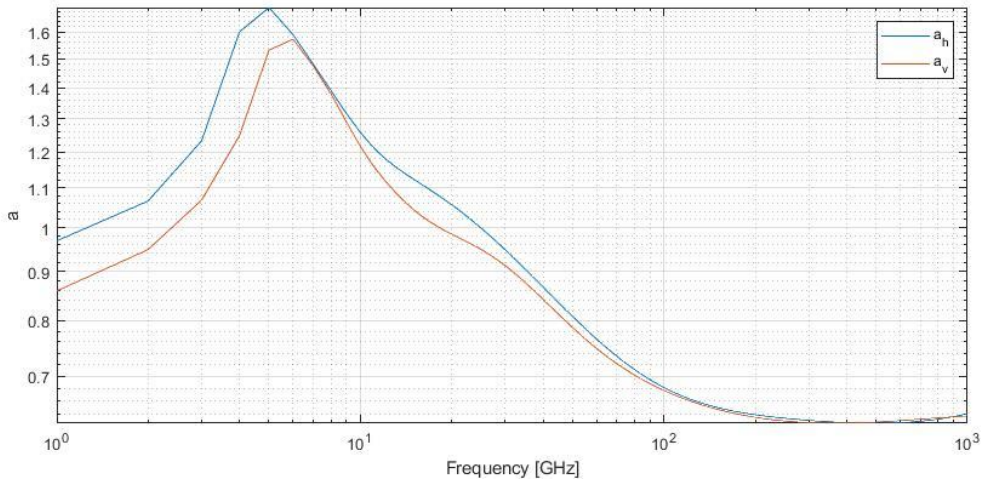

Figure 7: α^V and α^H coefficients for frequencies up to 1000 GHz

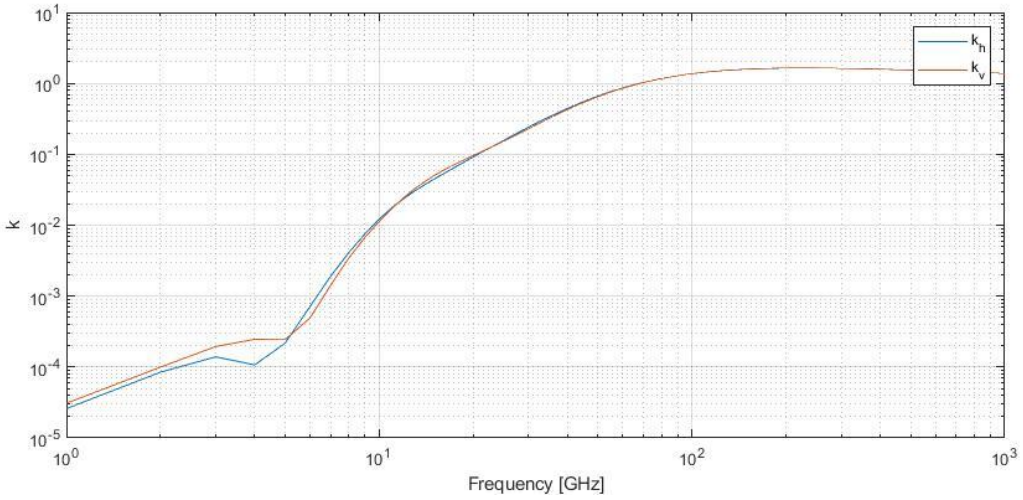

Figure 8: k^H and k^V coefficient for frequencies up to 1000 GHz

k and α can be computed from k^H, k^V, α^H and α^V with the following equations:

$$k = (k^H + k^V + (k^H - k^V)cos^2(\theta)\cos(2\tau))/2 \qquad (3.3.1.4)$$

$$\alpha = (k^H\alpha^H + k^V\alpha^V + (k^H\alpha^H - k^V\alpha^V)cos^2(\theta)\cos(2\tau)/2k \qquad (3.3.1.5)$$

where Θ is the link elevation angle and τ is the polarisation tilt angle relative to the horizontal. A polarisation tilt angle of 45° corresponds to a circular polarisation. If the polarisation is linear but τ is unknown, τ=45° offers a good compromise as well.

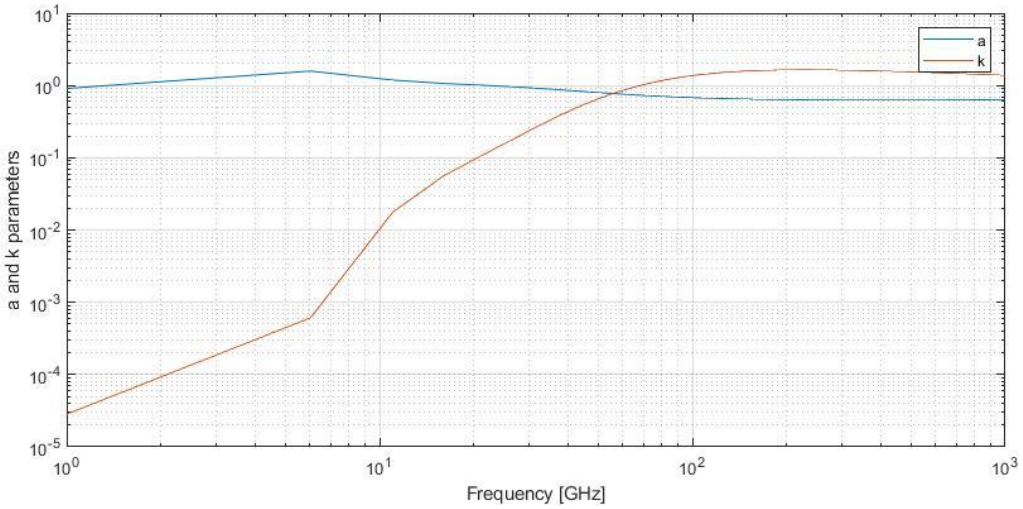

Figure 9: Coefficients α and k with a polarisation tilt angle of 45°

Once γ_{rain} is computed, the total rain attenuation along the path can be computed as:

$$A_{rain} = \int_0^L \gamma_{rain}(x)\, dx \quad (dB) \tag{3.3.1.6}$$

3.3.2 Rain rate from particle size distribution

To calculate the rain attenuation, the rain rate is needed. To do so, an important parameter to take into account when computing the rain rate is the Particle Size Distribution (PSD), or Drop Size Distribution (DSD). Indeed, according to the time spent in the cloud, the vertical movement in it and the ambient temperature, the drops have a very varied history and a distribution of diameters from a few micrometres to a few millimetres. As they fall, hydrometeors lose their spherical shape to become a flat ellipsoid because of the drag force of the air that tends to deform the drop. Liquid drops break out when the surface tension forces are not sufficient enough to maintain the cohesion. This implies that bigger drops have a shorter life.

The DSD has been widely studied and within a given volume of air, the number of drops for each diameter can be estimated statistically through a function referred as *N(D)* ($m^{-3}mm^{-1}$). In 1948, J. S. Marshall found out that the drop size distribution *N(D)* or number of drops per unit volume is often well modelled as an exponential law, written as (Marshall & Palmer, 1948):

$$N(D) = N_0 e^{-\Lambda D} \tag{3.3.2.1}$$

where *D* is the drop diameter, N_0 is the value of *N* when *D = 0,* $N_0 = 0.08\ cm^{-4}$ *and*

$$\Lambda = 41\ R^{-0.21} \qquad (cm^{-1}) \tag{3.3.2.2}$$

where *R* is the rate of rainfall in mm/hr.

However, the Marshall and Palmer distribution does not simulate properly drops of very small diameters. Several experiments have shown that the actual number of these droplets is less than the theoretical curve. In 1983, Carlton W. Ulbrich developed a more general formula taking into account that a drop is spherical if $D < 1\ mm$ and an ellipsoid whose horizontal axis gets flattened as *D* gets larger. The drop size distribution *N(D)* is then assumed to be a gamma distribution (Ulbrich, 1983).

$$N(D) = N_0 D^{\mu} e^{-\Lambda D} \tag{3.3.2.3}$$

For D (m) the diameter of the drop, μ the shape factor, and Λ (m^{-1}) the slope of the distribution. In general, for applications relative to signal attenuation, a simplified form of such function is considered, setting $\mu = 0$ and using $N_0 = 8 .\times 10^6\ m^{-3}m^{-1}$. The slope Λ is related to the mass of rain water per unit volume, or as well named rain water content for ERA5 data, M_{rain} ($kg\ m^{-3}$) (Quibus, 2020).

$$\Lambda = \left(\frac{\pi}{6}\frac{\rho_w}{M_{rain}} N_0 \Gamma(\mu + 4)\right)^{\frac{1}{\mu+4}} \tag{3.3.2.4}$$

with $\rho_w = 1000\ kg\ m^{-3}$ the density of water. The rain rate (mm/hr) can be computed as:

$$R = \frac{\pi}{6}\rho_w \int_{D_{min}}^{D_{max}} N(D) D^3 v(D)\ dD \tag{3.3.2.5}$$

where $v(D)$ is the terminal velocity of the drop of diameter D, and is assumed (Doviak & Zrnic, 1993) as:

$$v(D) = 3.778 D^{0.67} \quad \text{(in ms}^{-1}\text{ for } D \text{ in mm)} \tag{3.3.2.6}$$

3.3.3 Rain rate from ERA5 dataset

The rain rate can be obtained directly from ERA5 data, using the total column rain water, *tcrw* (kg/m^2). Since 1kg of water spread over 1 square metre of surface is 1mm deep (neglecting the effects of temperature on the density of water), therefore the units are equivalent to mm. Since the ERA5 data are given on an hourly basis, the total column rain water can be expressed in mm/hr. This parameter is a surface measurement, so a possibility is to assume that the ground value of the rain rate remains constant in altitude up to a certain level. As a rough approximation, the rain height can be assumed to be the 0°C isotherm (ITU-R, Recommendation ITU-R P.618-13, Propagation data and prediction methods required for the design of Earth-space telecommunication systems, 2017). This is not strictly correct, as liquid rain drops can exist above the freezing height, and so the rain attenuation is likely to be underestimated with this method. However, this method requires lot less computation time, and that is why it has been decided to also explore this method in addition to the DSD method to compute the rain attenuation.

3.4 Gas attenuation theory

At frequencies up to 1000 GHz, a part of the atmospheric attenuation is due to the atmospheric gases, especially oxygen and water. The spectrum of molecular oxygen is characterised by absorption lines at different frequencies, with a group of lines between 50 GHz and 70 GHz, and other isolated lines at 118.7 GHz and at frequencies higher than 300 GHz (Krupenie, 1972). The shape of theses absorption lines depends on the pressure and on the temperature. The attenuation due to water vapour is also characterised by absorption lines located at 22.23, 183 and 320 GHz, as well as other lines in millimetre waves and infrared. Their shape depends on the pressure and the temperature, like the oxygen, but also on the atmospheric water vapour content. The Recommendation ITU-R P.676-12 (ITU-R, Recommendation ITU-R P.676-12, Attenuation by atmospheric gases and related effects, 2019) allows to compute the attenuation by atmospheric gases on slant paths at different frequencies.

3.4.1 Specific attenuation

The specific attenuation can be accurately evaluated at any value of pressure, temperature and humidity as a summation of the individual spectral lines from oxygen and water vapour, together with small additional factors for the non-resonant Debye spectrum of oxygen below 10 GHz, pressure-induced nitrogen attenuation above 100 GHz and a wet continuum to account for the excess water vapour-absorption found experimentally. The specific gaseous attenuation is given by:

$$\gamma_{gas} = \gamma_o + \gamma_w = 0.1820 f \left(N_o''(f) + N_w''(f) \right) \quad \text{(dB/km)} \qquad (3.4.1.1)$$

where γ_o and γ_w are the specific attenuations (dB/km) due to dry air and water vapour respectively, f is the frequency (GHz) and $N_o''(f)$ and $N_w''(f)$ are the imaginary parts of the frequency-dependent complex refractivities:

$$N_o''(f) = \sum_{i\ (oxygen)} S_i F_i + N_D''(f) \qquad (3.4.1.2)$$

$$N_w''(f) = \sum_{i\ (water\ vapour)} S_i F_i \qquad (3.4.1.3)$$

S_i is the strength of the i^{th} oxygen or water vapour line, F_i is the oxygen or water vapour line shape factor, and the summations extend over all the spectral lines in Table 9 and

Table 10. $N_D''(f)$ is the dry continuum due to pressure-induced nitrogen absorption. All these contributions are given by:

$$N_D''(f) = f\ p\,\theta^2 \left[\frac{6.14 \times 10^{-5}}{d\left[1 + \left(\frac{f}{d}\right)^2\right]} + \frac{1.4 \times 10^{-12}\, p\,\theta^{1.5}}{1+1.9\times10^{-5}\ f^{1.5}} \right] \qquad (3.4.1.4)$$

where d is the width parameter for Debye spectrum, $d = 5.6\times10^{-4}(p+e)\theta^{0.8}$

$$S_i = a_1 \times 10^{-7} p\theta^3 \exp\left(a_2(1-\theta)\right) \qquad for\ oxygen \qquad (3.4.1.5)$$

$$S_i = b_1 \times 10^{-1} e\theta^{3.5} \exp\left(b_2(1-\theta)\right) \qquad for\ water\ vapour \qquad (3.4.1.6)$$

with p dry air pressure (hPa), e water vapour partial pressure (hPa), $\theta = 300/T$, T temperature (K). The water vapour partial pressure may be obtained from the water vapour density (g/m^3), using:

$$e = \frac{\rho T}{216.7} \qquad (3.4.1.7)$$

A way to compute the water vapour density is given in Recommendation ITU-R P.835-6:

$$\rho = \rho_0 \exp(-h/h_0) \qquad (3.4.1.8)$$

with the scale height $h_0 = 2km$ and the standard ground-level water vapour density is $\rho_0 = 7.5\ g/m^3$.

The dry air pressure p (hPa), is computed with: $p = P_{tot} - e$ (3.4.1.9)

The line shape factor is given by:

$$F_i = \frac{f}{f_i}\left[\frac{\Delta f - \delta\left(f_i - f\right)}{\left(f_i - f\right)^2 + \Delta f^2} + \frac{\Delta f - \delta\left(f_i + f\right)}{\left(f_i + f\right)^2 + \Delta f^2} \right] \qquad (3.4.1.10)$$

where f_i is the oxygen or water vapour line frequency and Δf is the width of the line:

$$\Delta f = a_3 \times 10^{-4}(p\theta^{(0.8-a_4)} + 1.1\ e\theta) \qquad for\ oxygen \qquad (3.4.1.11)$$

$$\Delta f = b_3 \times 10^{-4}(p\theta^{b_4} + b_5\ e\theta^{b_6}) \qquad for\ water\ vapour \qquad (3.4.1.12)$$

The line width is modified to account for Zeeman splitting of oxygen lines and Doppler broadening of water vapour lines:

$$\Delta f = \sqrt{\Delta f^2 + 2.25 \times 10^{-6}} \quad for\ oxygen \tag{3.4.1.13}$$

$$\Delta f = 0.535\Delta f + \sqrt{0.217\Delta f^2 + \frac{2.1316\times10^{-12} f_i^2}{\theta}} \quad for\ water\ vapour \tag{3.4.1.14}$$

δ is a correction factor that arises due to interference effects is oxygen lines:

$$\delta = (a_5 + a_6\theta) \times 10^{-4}(p+e)\theta^{0.8} \quad for\ oxygen \tag{3.4.1.15}$$

$$\delta = 0 \quad for\ water\ vapour \tag{3.4.1.16}$$

The coefficients *a* and *b* with respect to the absorption line frequencies are given in the following tables:

Table 9: Oxygen absoprtion lines parameters

f_0	a_1	a_2	a_3	a_4	a_5	a_6
50.474214	0.975	9.651	6.690	0.0	2.566	6.850
50.987745	2.529	8.653	7.170	0.0	2.246	6.800
51.503360	6.193	7.709	7.640	0.0	1.947	6.729
52.021429	14.320	6.819	8.110	0.0	1.667	6.640
52.542418	31.240	5.983	8.580	0.0	1.388	6.526
53.066934	64.290	5.201	9.060	0.0	1.349	6.206
53.595775	124.600	4.474	9.550	0.0	2.227	5.085
54.130025	227.300	3.800	9.960	0.0	3.170	3.750
54.671180	389.700	3.182	10.370	0.0	3.558	2.654
55.221384	627.100	2.618	10.890	0.0	2.560	2.952
55.783815	945.300	2.109	11.340	0.0	−1.172	6.135
56.264774	543.400	0.014	17.030	0.0	3.525	−0.978
56.363399	1331.800	1.654	11.890	0.0	−2.378	6.547
56.968211	1746.600	1.255	12.230	0.0	−3.545	6.451
57.612486	2120.100	0.910	12.620	0.0	−5.416	6.056
58.323877	2363.700	0.621	12.950	0.0	−1.932	0.436
58.446588	1442.100	0.083	14.910	0.0	6.768	−1.273
59.164204	2379.900	0.387	13.530	0.0	−6.561	2.309
59.590983	2090.700	0.207	14.080	0.0	6.957	−0.776
60.306056	2103.400	0.207	14.150	0.0	−6.395	0.699
60.434778	2438.000	0.386	13.390	0.0	6.342	−2.825
61.150562	2479.500	0.621	12.920	0.0	1.014	−0.584
61.800158	2275.900	0.910	12.630	0.0	5.014	−6.619
62.411220	1915.400	1.255	12.170	0.0	3.029	−6.759
62.486253	1503.000	0.083	15.130	0.0	−4.499	0.844
62.997984	1490.200	1.654	11.740	0.0	1.856	−6.675
63.568526	1078.000	2.108	11.340	0.0	0.658	−6.139
64.127775	728.700	2.617	10.880	0.0	−3.036	−2.895
64.678910	461.300	3.181	10.380	0.0	−3.968	−2.590
65.224078	274.000	3.800	9.960	0.0	−3.528	−3.680
65.764779	153.000	4.473	9.550	0.0	−2.548	−5.002
66.302096	80.400	5.200	9.060	0.0	−1.660	−6.091
66.836834	39.800	5.982	8.580	0.0	−1.680	−6.393
67.369601	18.560	6.818	8.110	0.0	−1.956	−6.475
67.900868	8.172	7.708	7.640	0.0	−2.216	−6.545
68.431006	3.397	8.652	7.170	0.0	−2.492	−6.600
68.960312	1.334	9.650	6.690	0.0	−2.773	−6.650
118.750334	940.300	0.010	16.640	0.0	−0.439	0.079
368.498246	67.400	0.048	16.400	0.0	0.000	0.000
424.763020	637.700	0.044	16.400	0.0	0.000	0.000
487.249273	237.400	0.049	16.000	0.0	0.000	0.000
715.392902	98.100	0.145	16.000	0.0	0.000	0.000
773.839490	572.300	0.141	16.200	0.0	0.000	0.000
834.145546	183.100	0.145	14.700	0.0	0.000	0.000

Table 10: Water vapour absorption line parameters

f_0	b_1	b_2	b_3	b_4	b_5	b_6
22.235080	0.1079	2.144	26.38	0.76	5.087	1.00
67.803960	0.0011	8.732	28.58	0.69	4.930	0.82
119.995940	0.0007	8.353	29.48	0.70	4.780	0.79
183.310087	2.273	0.668	29.06	0.77	5.022	0.85
321.225630	0.0470	6.179	24.04	0.67	4.398	0.54
325.152888	1.514	1.541	28.23	0.64	4.893	0.74
336.227764	0.0010	9.825	26.93	0.69	4.740	0.61
380.197353	11.67	1.048	28.11	0.54	5.063	0.89
390.134508	0.0045	7.347	21.52	0.63	4.810	0.55
437.346667	0.0632	5.048	18.45	0.60	4.230	0.48
439.150807	0.9098	3.595	20.07	0.63	4.483	0.52
443.018343	0.1920	5.048	15.55	0.60	5.083	0.50
448.001085	10.41	1.405	25.64	0.66	5.028	0.67
470.888999	0.3254	3.597	21.34	0.66	4.506	0.65
474.689092	1.260	2.379	23.20	0.65	4.804	0.64
488.490108	0.2529	2.852	25.86	0.69	5.201	0.72
503.568532	0.0372	6.731	16.12	0.61	3.980	0.43
504.482692	0.0124	6.731	16.12	0.61	4.010	0.45
547.676440	0.9785	0.158	26.00	0.70	4.500	1.00
552.020960	0.1840	0.158	26.00	0.70	4.500	1.00
556.935985	497.0	0.159	30.86	0.69	4.552	1.00
620.700807	5.015	2.391	24.38	0.71	4.856	0.68
645.766085	0.0067	8.633	18.00	0.60	4.000	0.50
658.005280	0.2732	7.816	32.10	0.69	4.140	1.00
752.033113	243.4	0.396	30.86	0.68	4.352	0.84
841.051732	0.0134	8.177	15.90	0.33	5.760	0.45
859.965698	0.1325	8.055	30.60	0.68	4.090	0.84
899.303175	0.0547	7.914	29.85	0.68	4.530	0.90
902.611085	0.0386	8.429	28.65	0.70	5.100	0.95
906.205957	0.1836	5.110	24.08	0.70	4.700	0.53
916.171582	8.400	1.441	26.73	0.70	5.150	0.78
923.112692	0.0079	10.293	29.00	0.70	5.000	0.80
970.315022	9.009	1.919	25.50	0.64	4.940	0.67
987.926764	134.6	0.257	29.85	0.68	4.550	0.90
1780.000000	17506.0	0.952	196.3	2.00	24.15	5.00

3.4.2 Slant path attenuation

For an Earth-Space slant path, the gaseous attenuation can be calculated with:

$$A_{gas} = \int_{h_1}^{h_2} \frac{\gamma_{gas}(h)}{sin\ \varphi(h)}\, dh = \int_{h_1}^{h_2} \frac{\gamma_{gas}(h)}{\sqrt{1-cos^2\varphi(h)}}\, dh \qquad (dB) \tag{3.4.2.1}$$

$$\cos\varphi(h) = \frac{(R_E+h_1)n(h_1)}{(R_E+h)n(h)}\cos(\varphi_1) \tag{3.4.2.3}$$

where $\gamma_{gas}(h)$ is the specific attenuation at height h, $R_E = 6371\ km$ is the average Earth radius, $n(h)$ is the refractive index at height h, and φ_1 is the local apparent elevation angle at height h_1. Since the Earth is considered flat in the area of study, the local apparent elevation angle φ_1 is the same at any height, and $\varphi_1 = 35.42°$.

To compute the refractive index $n(h)$, the Recommendation ITU-R P.453-14 was used.

$$n = 1 + N \times 10^{-6} \tag{3.4.2.4}$$

with the radio refractivity N:

$$N = 77.6\frac{p}{T} + 72\frac{e}{T} + 3.75 \times 10^5\frac{e}{T^2} \tag{3.4.2.3}$$

4 RESULTS

4.1 Attenuation by clouds with ERA5 data

Following the Recommendation IUT-R P.840-8, the cloud attenuation has been computed using the data from ERA5. First, the specific attenuation coefficient K_l $[(\mathrm{dB/km})/(\mathrm{g/m^3})]$ was calculated using equation (3.2.1.2):

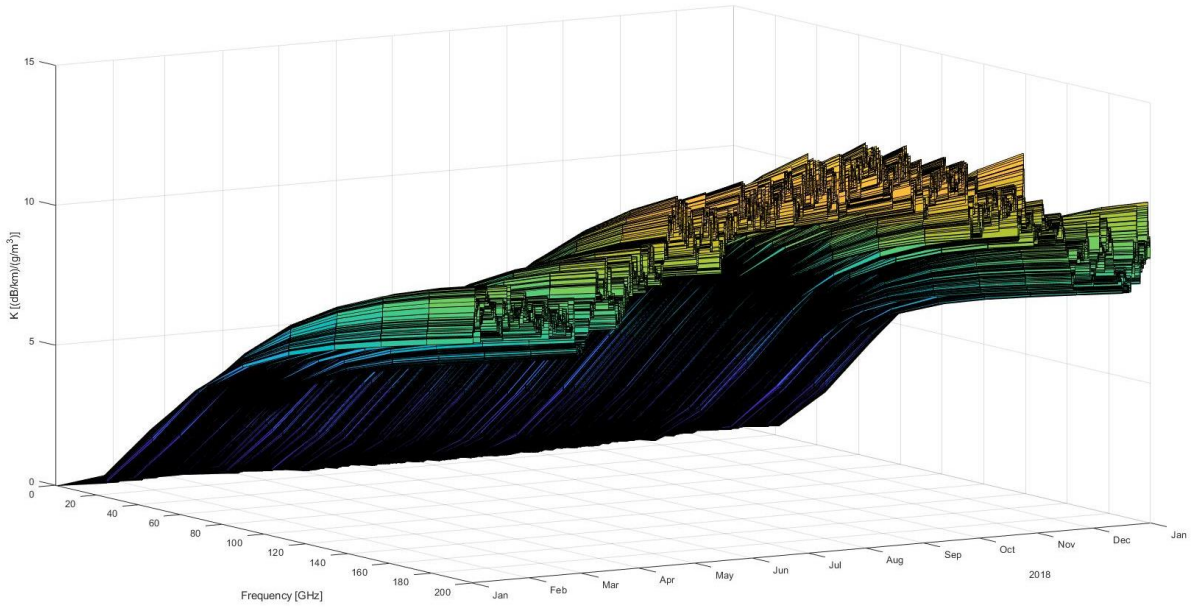

Figure 10: K_l as a function of the frequency over the year 2018, for pixel 2 at 169 m.

As it can be seen in Figure 10, the values of K_l increase with the frequency and tend to be higher in summer than in winter. This frequency-temperature dependency can be well seen in the following Figure 11:

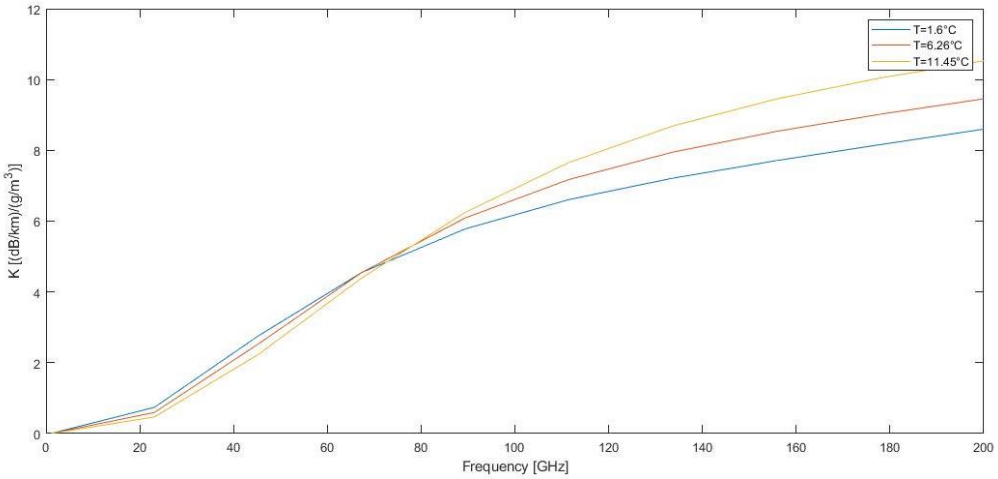

Figure 11: K_l as a function of the frequency for several temperatures during the month of January 2018 for pixel 2 at 169 m a.m.s.l.

Using the liquid water density *M* shown in Figure 12, the cloud attenuation along the slant path over the year can be calculated for the two frequencies of interest.

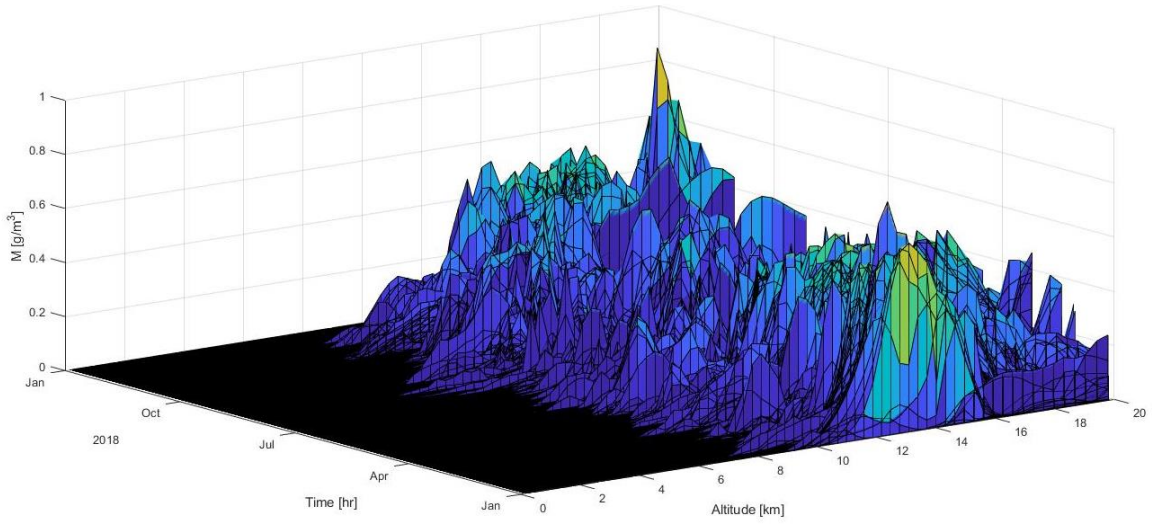

Figure 12: Liquid water density in the cloud M as a function of the altitude and time, for pixel 2

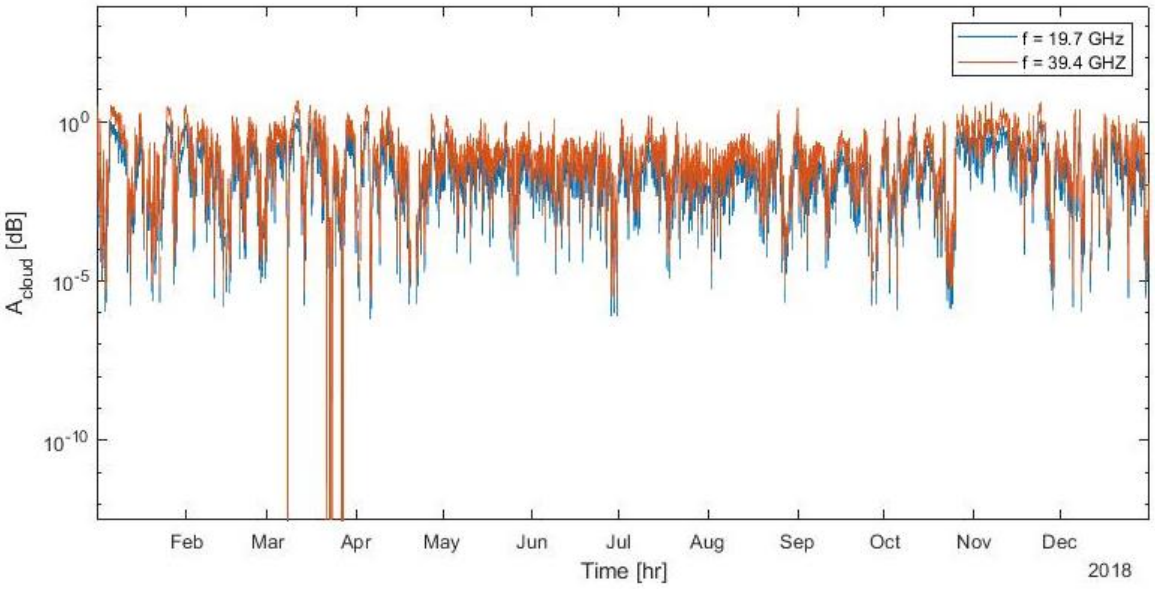

Figure 13: Cloud attenuation (dB) along the path as a function of time, for two frequencies 19.7 GHz and 39.4 GHz

The cloud attenuation seems to not really depend on the month of the year. So an average value over the year was calculated: for f=19.7 Ghz, $A_{cloud} = 0.0708\, dB$, and for f=39.4 GHz, $A_{cloud} = 0.2258\, dB$. The maximum values reached are $A_{cloud,max} = 1.2593\, dB$ at 19.7 GHz, and $A_{cloud,max} = 4.6519\, dB$ at 39.4 GHz. As it can be seen in the figure above, A_{cloud} increases with the frequency.

Between Mars and April 2018, some discontinuities are present: according to the documentation of ERA5, this dataset is produced by several parallel experiments, each for a different period, which are then appended together to create the final product. This can create discontinuities at the transition points.

The accuracy of the cloud attenuation derived from ERA5 data has been studied by analysing the annual Complementary Cumulative Distribution Function (CCDF). The CCDF curves in the whole 2018 are shown in Figure 14 by comparing at 19.7 and 39.4 GHz, the cloud attenuation computed using the ERA5 dataset, and real measurements. These measurements come directly from Alphasat data in Milan in 2018.

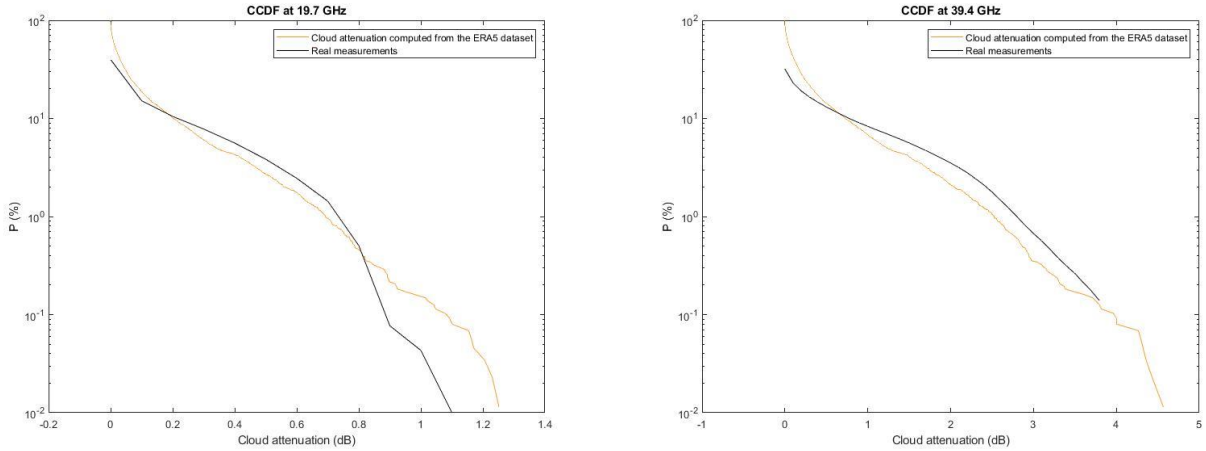

Figure 14: Cloud attenuation CCDF

At 19.7 GHz, from 0 to 0.8 dB, and at 39.4 GHz, from 0 to 3.8 dB, the cloud attenuation computed with the ERA5 dataset seems to be in quite good agreement with the real measurements. However, higher values of attenuation are reached using the ERA5 dataset. This is likely due to the cloud liquid water content that is used to compute M in (3.2.1.1). Indeed, the integrated cloud liquid water content presents quite high peak values reaching 4 mm.

4.2 Attenuation by rain with ERA5 data

In order to compute the rain attenuation, the rain rate was first needed to be calculated since it was not available in the ERA5 dataset. To do so, two different methods were used. The first one is using the Drop Size Distribution theory, as explained in section 3.3.2. This method asks for a longer calculation time and capacity due to the different integrations. The second method, as described in section 3.3.3 was also used to compute the rain attenuation over the entire year. This method is faster, but less accurate.

Starting with the first method, from the specific rain water content q (kg/kg) and from the dry air density ρ_{air} (kg/m^3), the density of rain water M_{rain} (kg/m^3) can be simply obtained as:

$$M_{rain} = q\rho_{air} \tag{4.2.1}$$

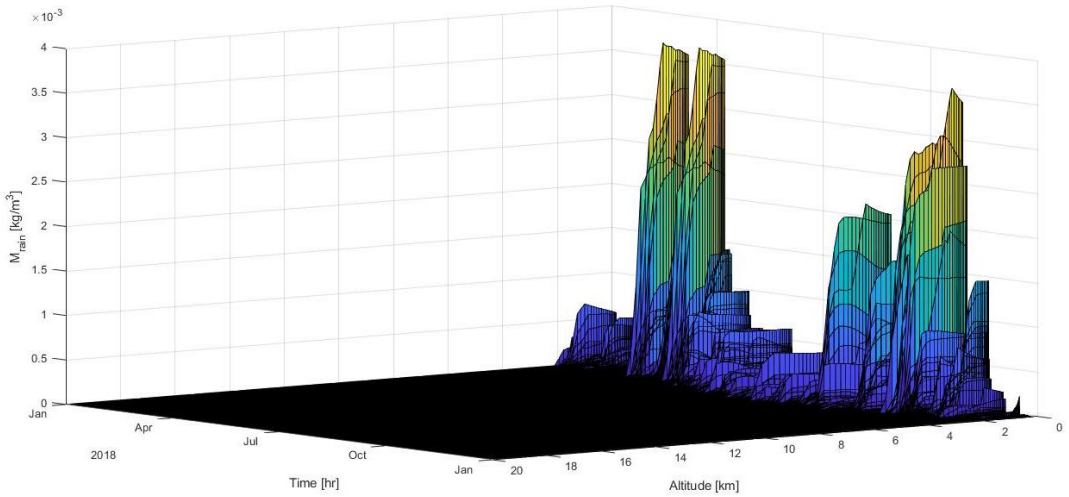

Figure 15: Density of rain water (kg/m³) over the year for pixel 2

Then, using equation (3.3.2.4) to get Λ, the number of drops per unit volume *N(D)* can be computed with equation (3.3.2.3), where D the drop diameter is a vector containing values from 0 to 4 mm. The choice of $D_{max} = 4\ mm$ is well supported by looking the Figure 17. Indeed, for a Marshall-Palmer distribution, the number of drops becomes negligible after a drop size D_{max}.

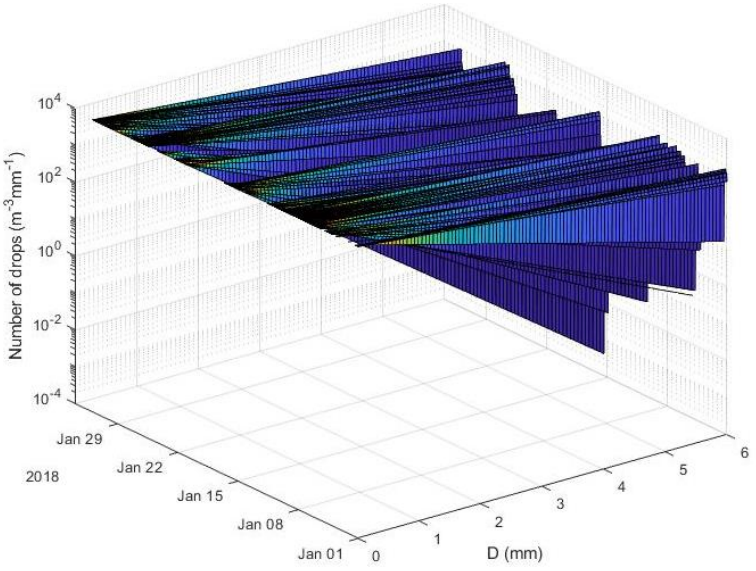

Figure 16: Number of drops during the month of January 2018 for pixel 2 according to their diameter

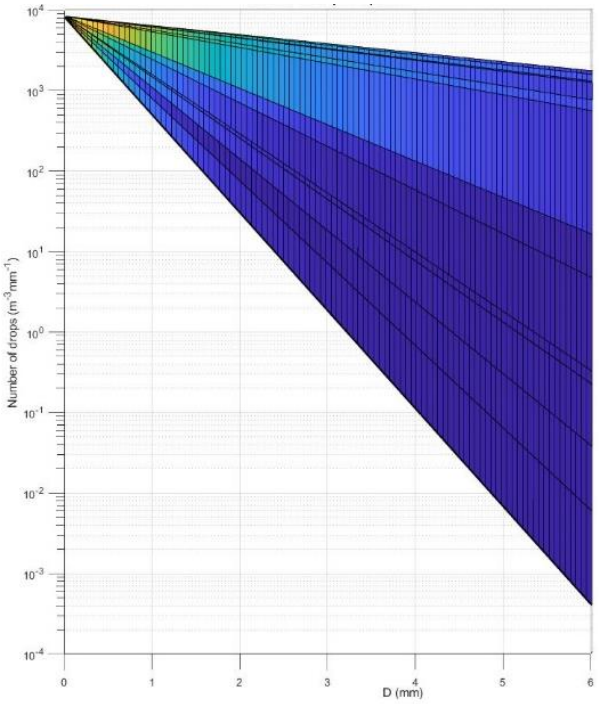

Figure 17: Number of drops during the month of January 2018, for pixel 2

Finally, using the equation (3.3.2.5), the rain rate R (mm/hrs) can be calculated by an integration over the drop diameter D (mm). In the Figure 18, the rain rate R is plotted for each hours of the year 2018.

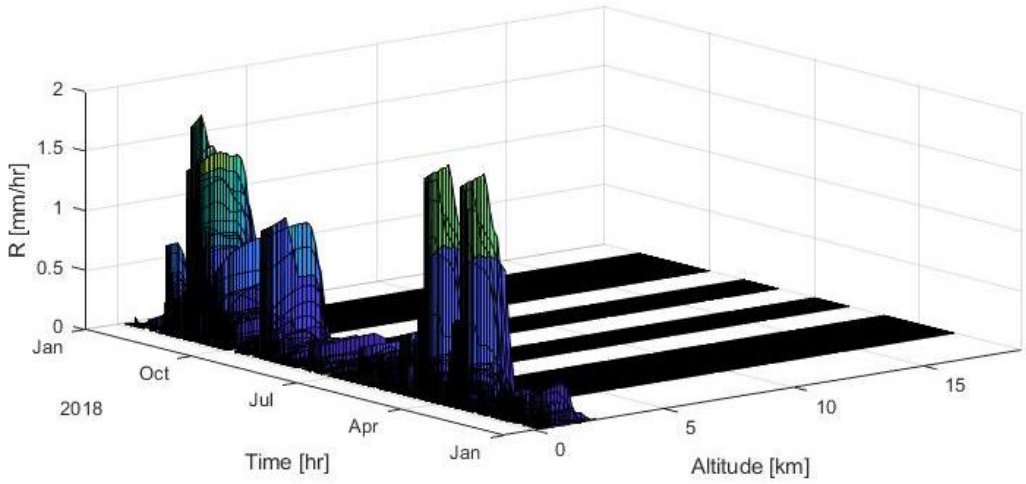

Figure 18: Rain rate over the year for pixel 2 as function of the altitude

Once the rain rate is obtained, the specific rain attenuation γ_{rain} in (dB/km) is computed with equation (3.3.1.1):

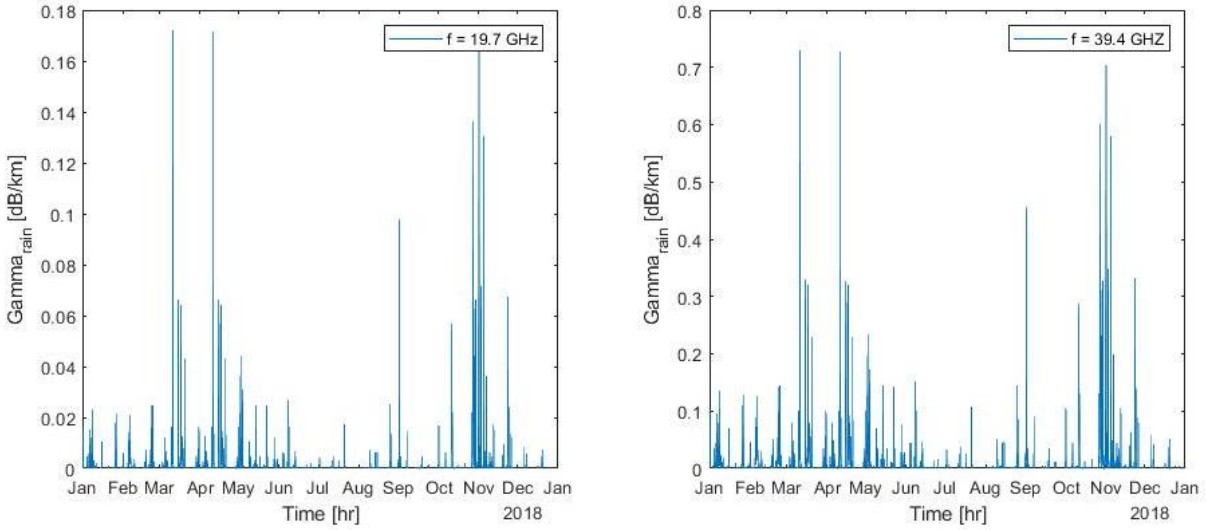

Figure 19: Gamma$_{rain}$ (dB/km) over the year for pixel 2 and for the two frequencies of interest

By performing an integration over the effective length of the path, the rain attenuation A_{rain} (dB) over the year was computed.

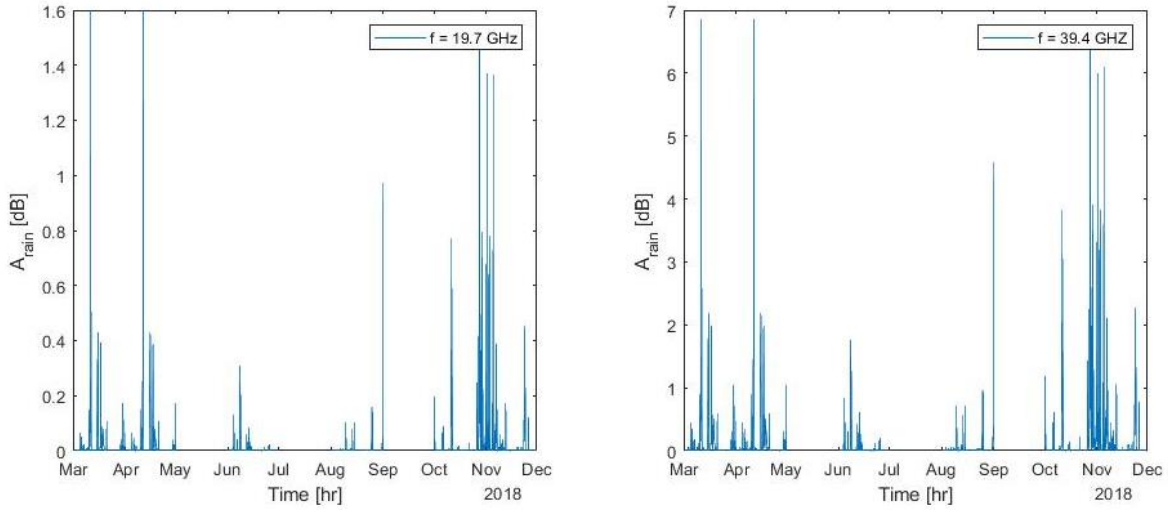

Figure 20: Rain attenuation (dB) over the year

Using the second method, as described in section 3.3.3, the rain rate is directly retrieved from the ERA5 dataset. The following figure shows it over the year:

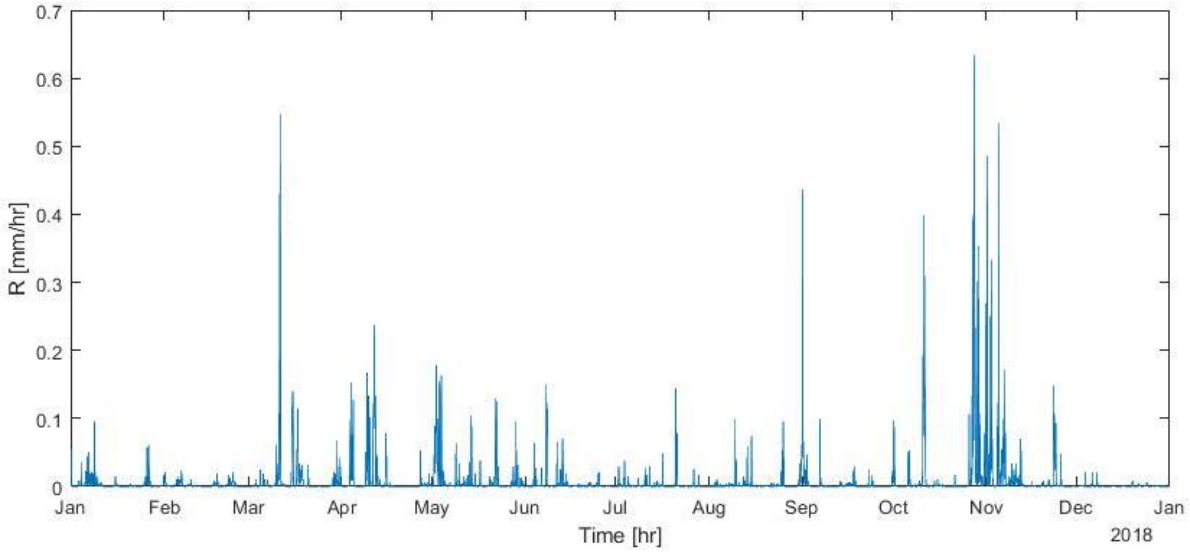

Figure 21: Rain rate over the year for pixel 2

When comparing the two different methods to compute the rain attenuation, it comes out that using the DSD method, the rain rate has peak values higher (Figure 18) than using the second method (Figure 21). It is certainly due to the fact that the assumption made for the second method is quite rough. Indeed, considering the rain height to be the 0°C isotherm is not strictly correct since liquid drops can exist above this height.

Knowing the rain rate, the specific rain attenuation γ_{rain} (dB/km) and the rain attenuation A_{rain} (dB) were computed at the two frequencies of interest:

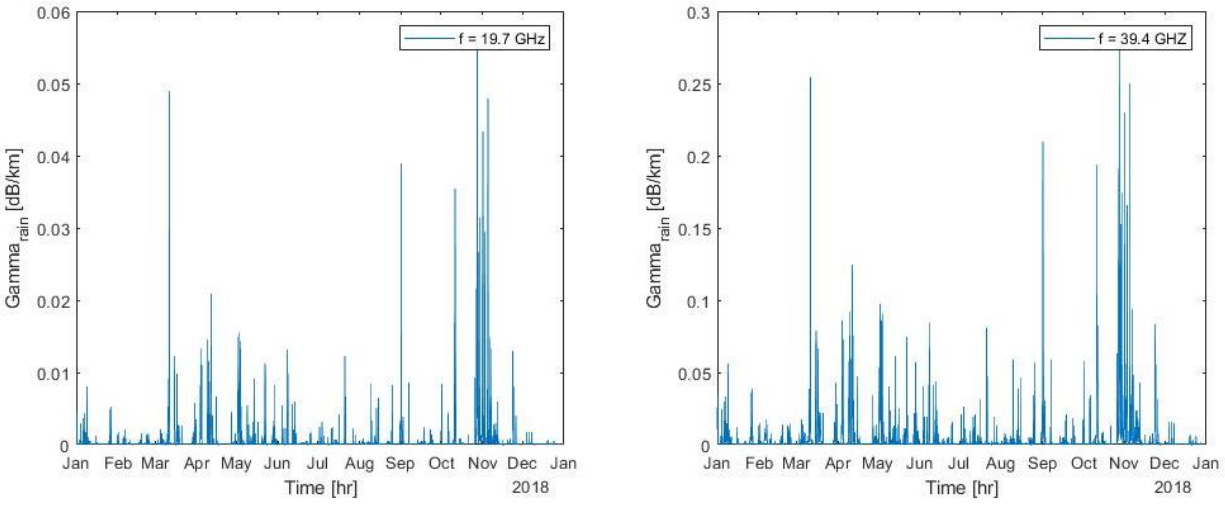

Figure 22: Specific rain attenuation (dB/km) for pixel 2 over the year

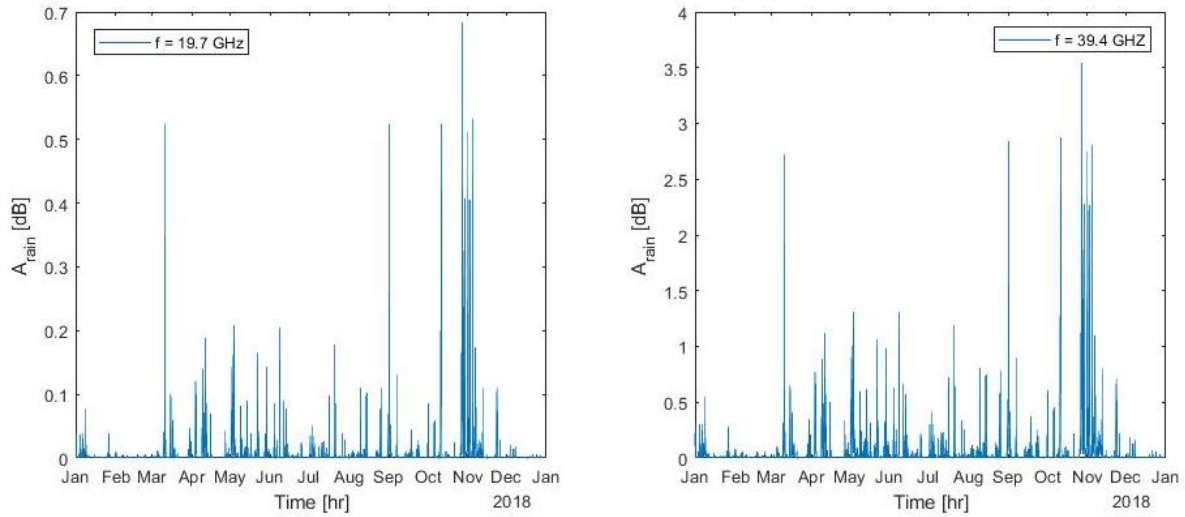

Figure 23: Rain attenuation (dB) over the year

Finally, Figure 24 shows the comparison between the two methods where the rain rate was calculated with the DSD theory, or directly retreived from the ERA5 dataset.

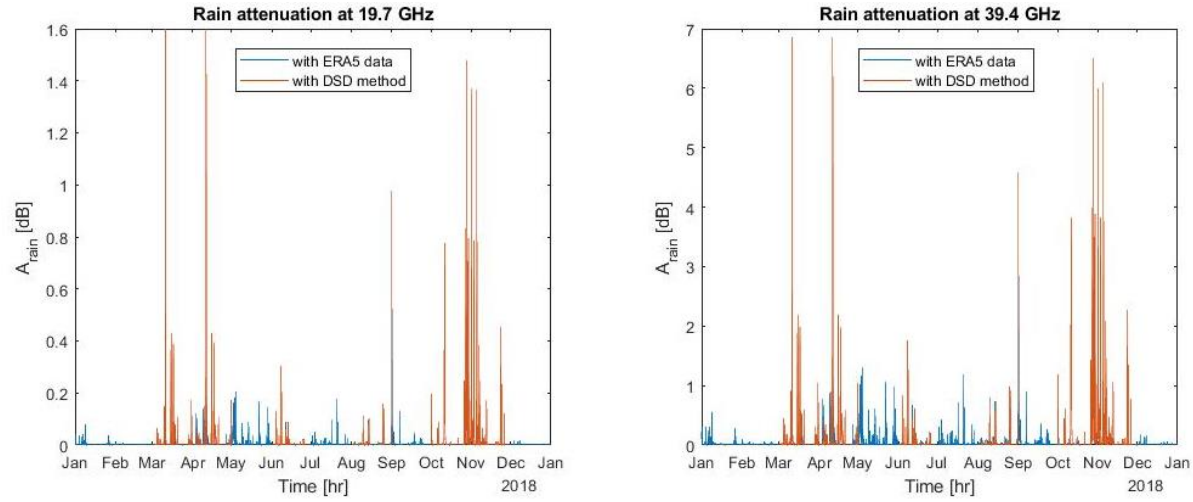

Figure 24: Rain attenuation (dB) over the year for the two methods

It can be seen that the DSD method offers higher attenuation values then when the rain is directly retrieved from the ERA dataset.

The CCFD of the rain attenuation was also computed to compare the two methods with real measurements. In the Figure 25, the method 1 is when the rain rate is directly retrieved from the ERA5 dataset, and the method 2 is using the DSD theory to compute *R*.

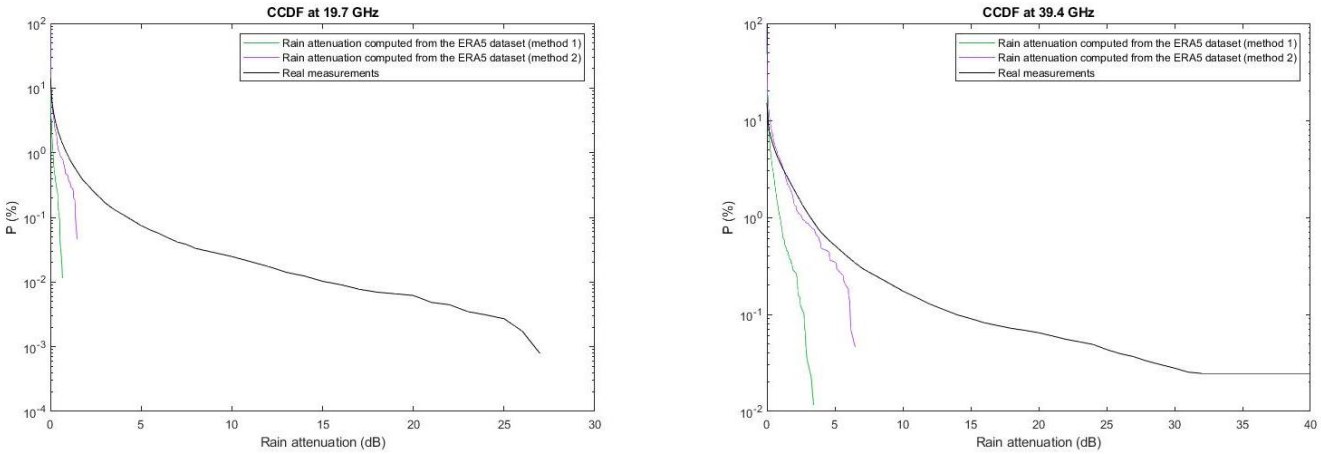

Figure 25: Rain attenuation CCDFs

As expected, due to the very low achieved rain rates, the rain attenuation is highly underestimated by using the ERA5 dataset. Even though when using the DSD higher rain attenuation values are obtained, the prediction performance is quite limited. This is lekily due to the limited spatial and temporal resolutions of the ERA5 dataset, which are not sufficient to properly catch the fast evolution and localized nature of rainfall events.

4.3 Attenuation by gas with ERA5 data

Following the Recommendation ITU-R P.676-12, as explained in section 3.4.1, the attenuation due to atmospheric gases can be computed, using ERA5 data. First, the specific gaseous attenuation γ_{gas} (dB/km) was computed using equation (3.4.1.1).

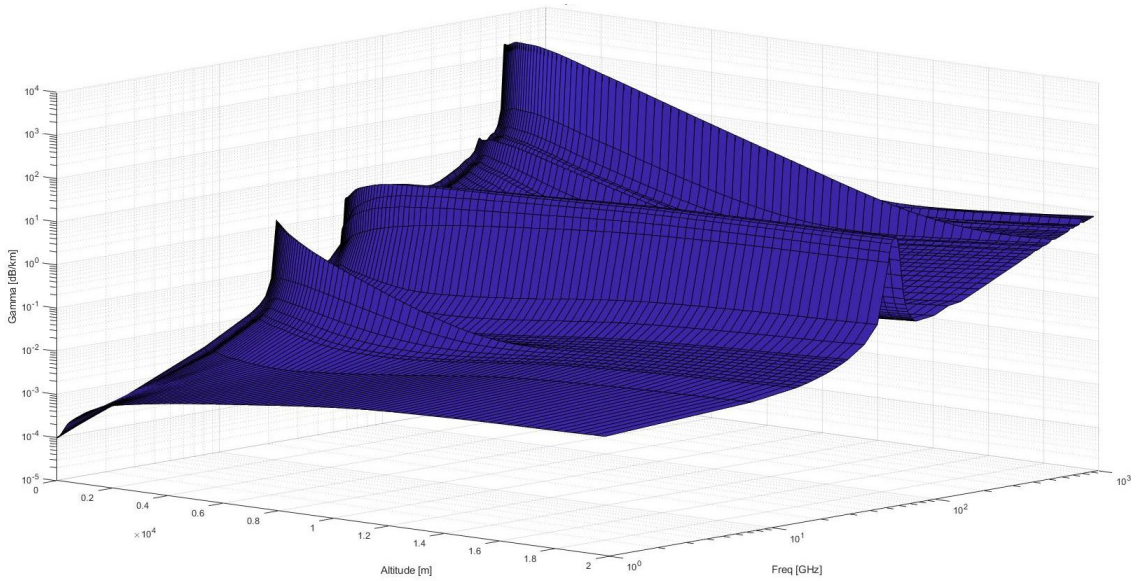

Figure 26: γ_{gas} (dB/km) for pixel 2, for the month of January 2018

As it is observed in Figure 26, there is a water vapour absorption peak at 22.2 GHz and around 183 GHz, and an oxygen absorption peak around 60 GHz. However this figure shows very well that the water vapour absorption peak amplitude is not constant with altitude. This peak is present only for altitudes from 0 to 10 km.

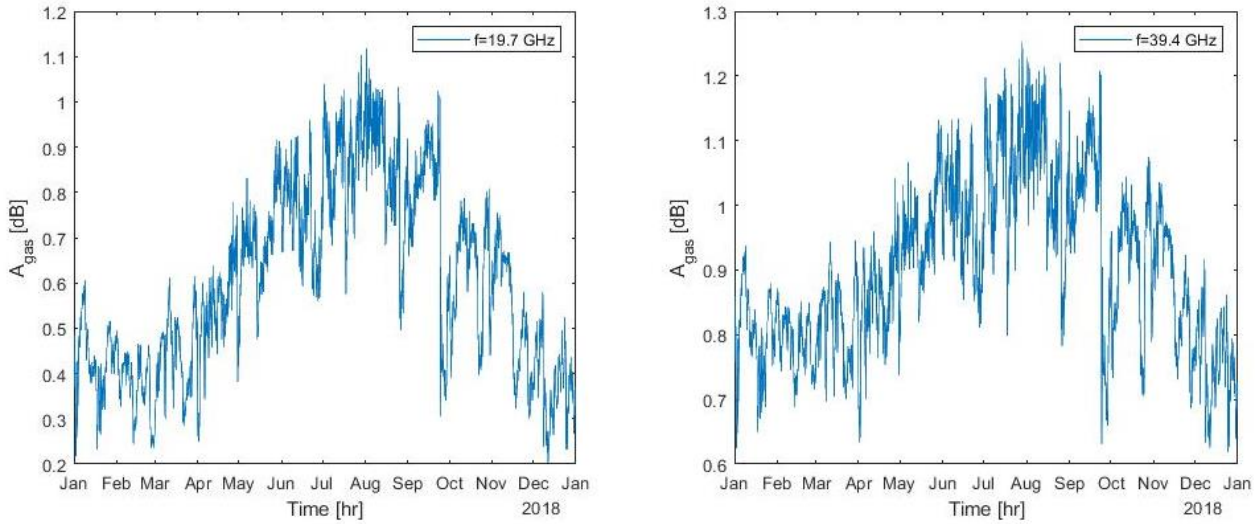

Figure 27: Gas attenuation (dB) over the year for f=19.7 GHz and f=39.4 GHz

The atmospheric gas attenuation varies in function of the time of the year. The Figure 27 shows that the attenuation is maximum in summer (for the month of August), and minimum in winter. It is due to the strong dependence on the density of water vapour, whose profile is given in Figure 28:

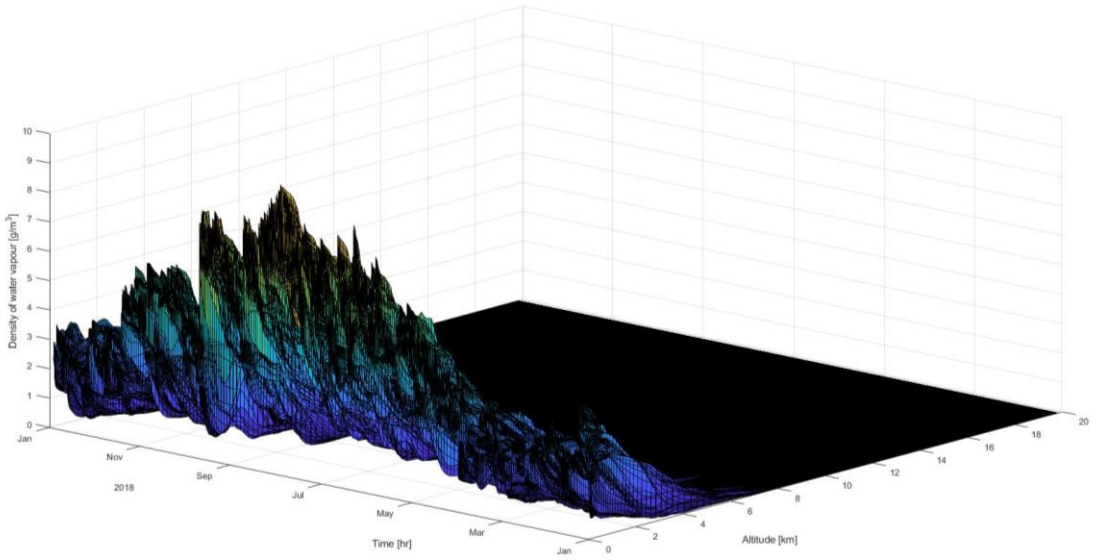

Figure 28: Density of water vapour for the pixel 2

Finally, the CCDF of the gas attenuation was computed in Figure 29:

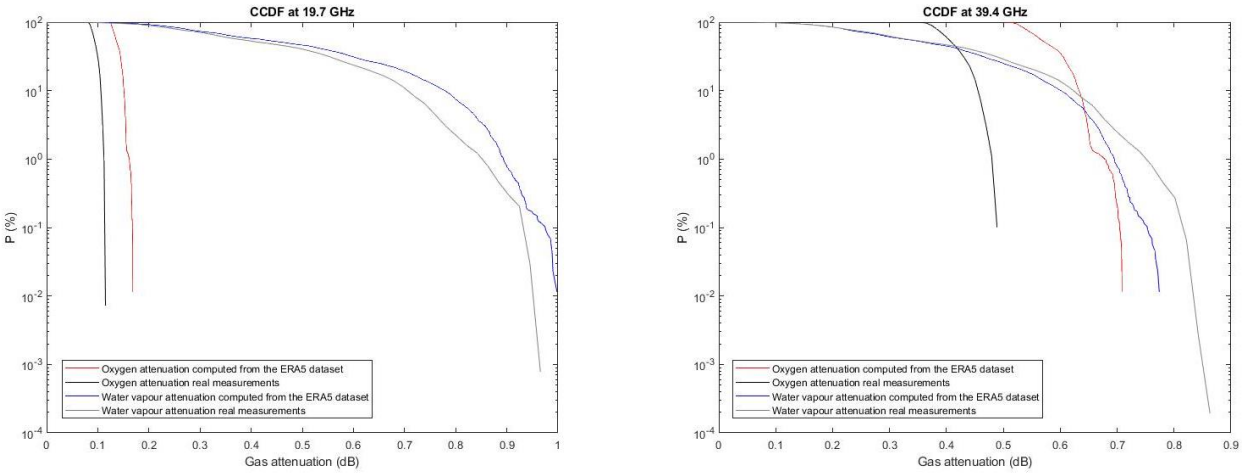

Figure 29: Gas attenuation CCDFs

At 19.7 GHz the oxygen and water vapour attenuations computed with the ERA5 dataset tend to follow the real measurements, even though computed values seem to be a slightly higher. At 39.4 GHz, an overestimation of the oxygen attenuation can be noticed, though in the order of tenths of dB. Instead of being between 0.36 dB - 0.49 dB, values range from 0.52 dB to 0.7 dB.

4.4 Total attenuation

Finally, after computing all the different types of attenuation, the total attenuation over the year can be calculated as:

$$A_{total} = A_{cloud} + A_{rain} + A_{gas} \tag{4.4.1}$$

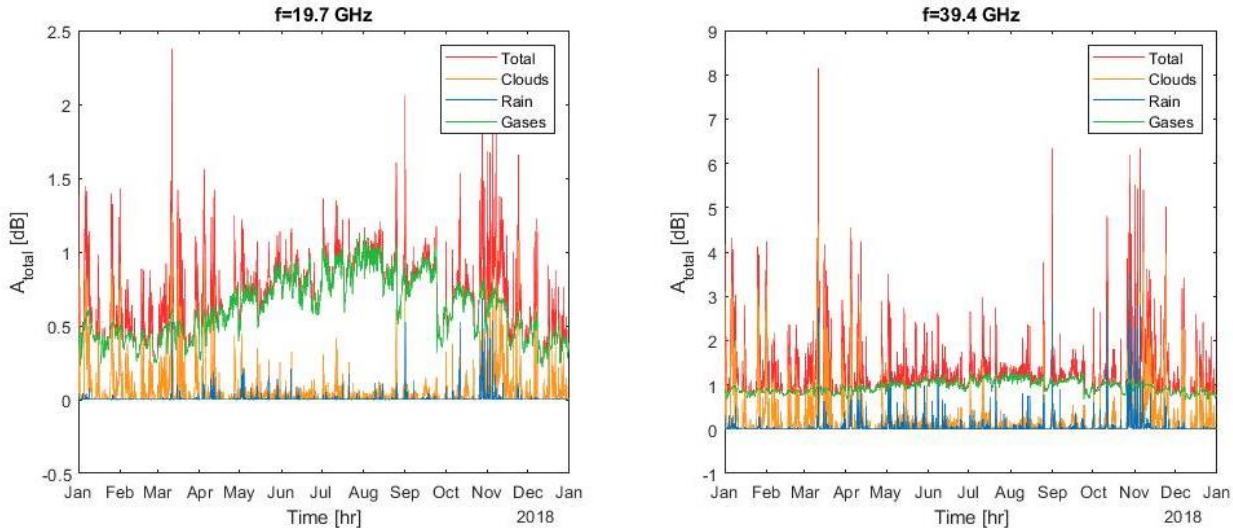

Figure 30: Total attenuation (dB) over the year with the rain rate retrieved from the ERA5 dataset

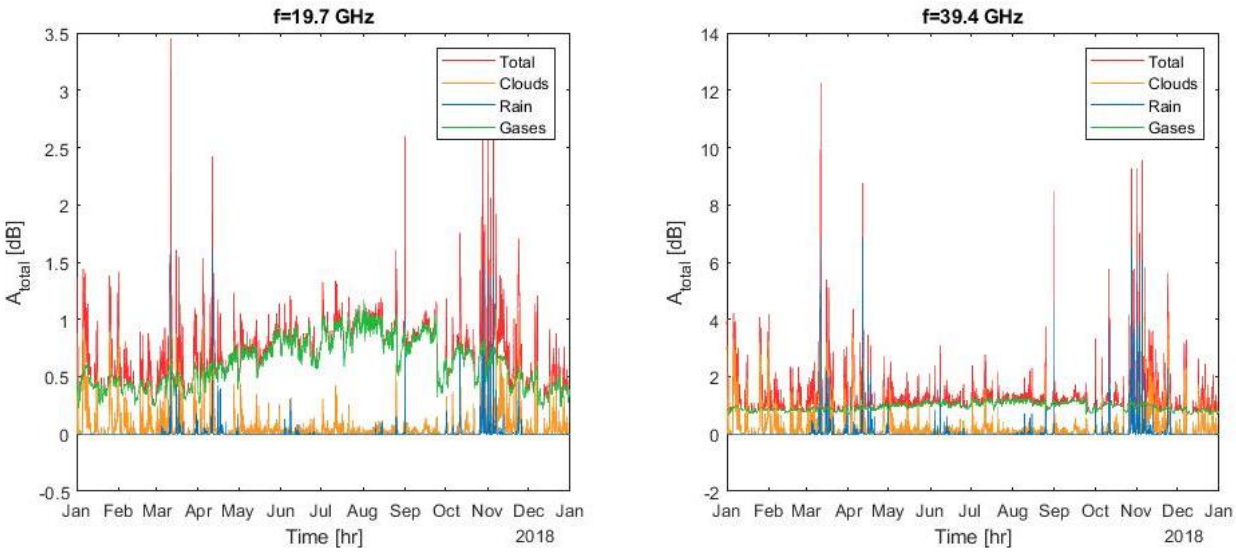

Figure 31: Total attenuation (dB) over the year using the DSD theory for the rain rate

The CCDF curves were also computed as it can be seen in Figure 32 and Figure 33:

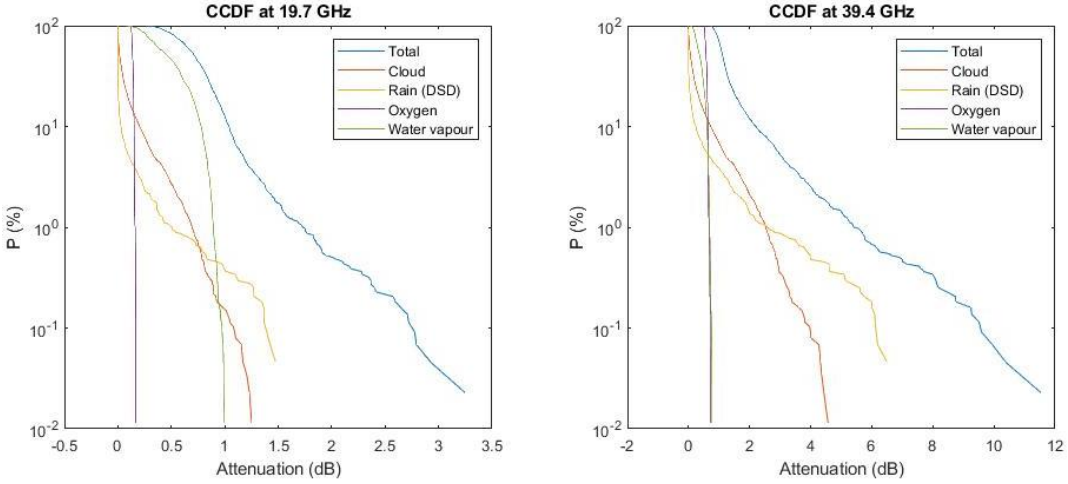

Figure 33: Total attenuation CCDF, with the rate rate computed with the DSD theory

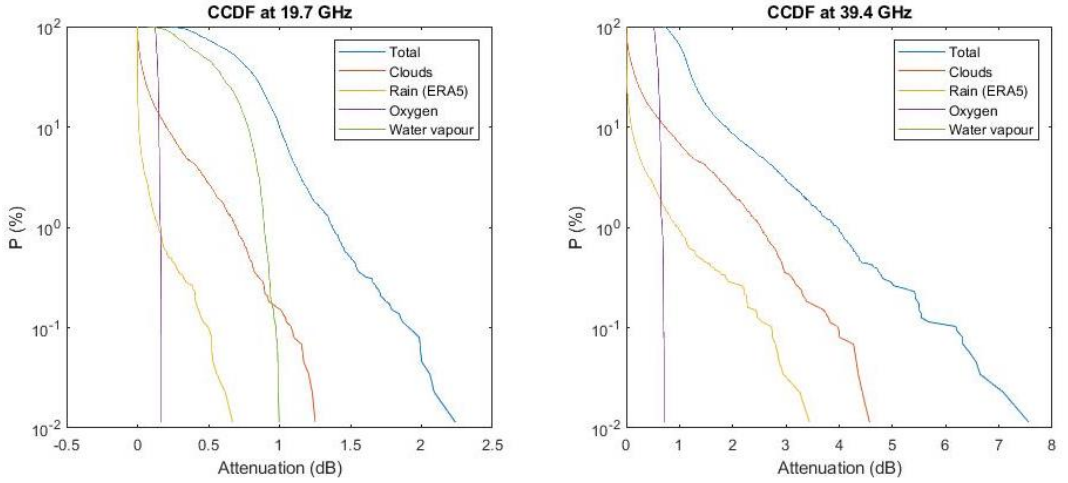

Figure 32: Total attenuation CCDF, with the rain rate retrieved from ERA5 dataset

Finally, in order to asses the accuracy of the computed attenuations, the CCDF of the total attenuation was compared with the one obtained with the Alphasat data in 2018.

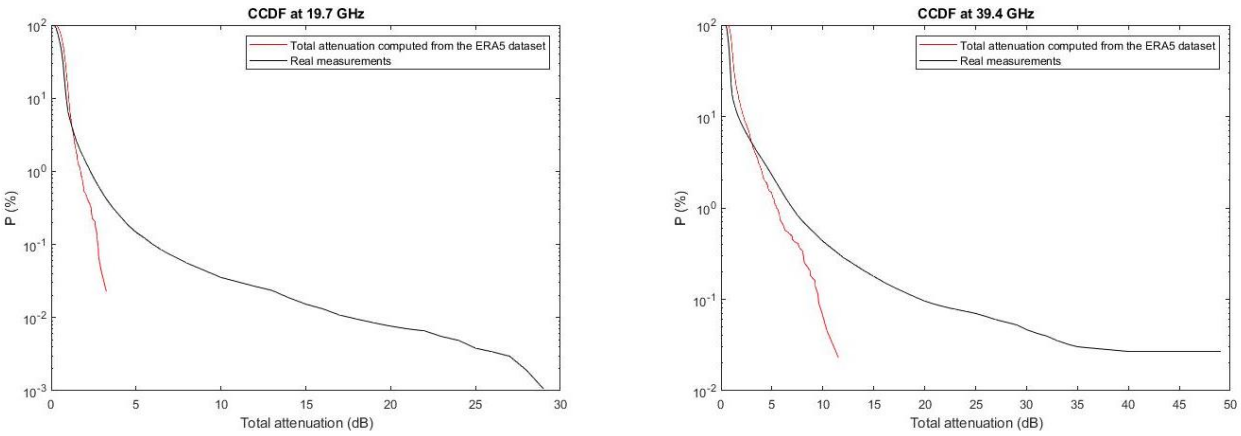

Figure 34: Total attenuation CCDF from real measurements and total attenuation CCDF with R computed with the DSD theory

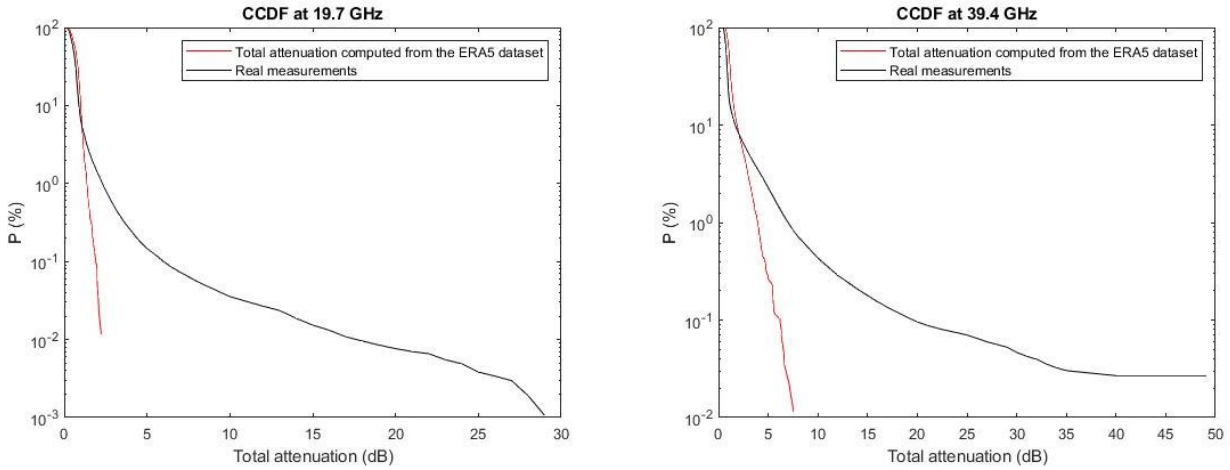

Figure 35: Total attenuation CCDF from real measurements and total attenuation CCDF with R retrieved from the ERA5 dataset

When the probability is high, i.e. when the total attenuation is low ($A_{total} < 2\ dB$ at 19.7 GHz and $A_{total} < 4\ dB$ at 39.4 GHz for Figure 34, $A_{total} < 1.1\ dB$ at 19.7 GHz and $A_{total} < 2.1\ dB$ at 39.4 GHz for Figure 35), the attenuation computed with the ERA5 dataset agrees quite well the one obtained with real measurements. However, for lower probabilities, the computed total attenuation is largely underestimated. Since the computed cloud, and gas attenuations match pretty well the real measurements (they even tends to be a little bit higher than the real measurements), it can be deduced that it is certainly due to the rain attenuation, which is way below the attenuation computed with the Alphasat data.

5 FINAL REMARKS & PERSPECTIVES

This work investigated the main tropospheric effects affecting Earth-space links, using the ERA5 data. Specifically, the link between the Alphasat satellite and a ground station in Milan (Italy) was studied at two frequencies, 19.7 and 39.4 GHz. Since ERA5 is the latest climate reanalysis produced by the ECMWF, the objective of this thesis was to asses if and to what extent this new reanalysis could be used to directly evaluate the tropospheric impairments affecting mm-waves. First, in order to download a limited amount of data from the ERA5 dataset, an area of study was defined and the path of the signal was identified and discretized. Then, following the ITU-R Recommendations, the cloud, rain and gaseous attenuations were computed over the year of 2018.

The cloud attenuation A_{cloud} (dB) seemed to not depend on the month of the year. The maximum values reached are $A_{cloud,max} = 1.2593\ dB$ at 19.7 GHz, and $A_{cloud,max} = 4.6519\ dB$ at 39.4 GHz. These values are a little bit higher than expected, but this can be explained by the cloud liquid water content, directly retrieved from the ERA5 dataset, which is used to computed the cloud attenuation and which is also higher than expected. When comparing the CCDF curve of the computed cloud attenuation with the CCDF curve obtained with real measurements coming from Alphasat, it came out that the two curves seem to match pretty well, except for high attenuation values.

In order to compute the rain attenuation, the rain rate was needed. To this aim, two methods were used. The first one uses the DSD theory. The rain rate was retrieved from an integration over the drop diameter and using the density of rain water M_{rain} (kg/m^3). The density of rain water was compute thanks to the specific rain water content q (kg/kg), directly downloaded from the ERA5 dataset. The computed rain rate reaches values that are a little bit low (around 1.5-2 mm/hr). The second method uses the total column rain water (kg/m^2), retrieved from the ERA5 data, which is equivalent to the rain rate R (mm), assuming that the ground value of the rain rate remains constant in altitude up to the 0°C isotherm height. This is a rough approximation, but this method requires less computation time. With these methods the rain rate was even lower, reaching values around 0.6-0.7 mm/hr. From the rain rate, the rain attenuation A_{rain} (dB) and the

associated CCDF can be computed. It came out that using the second method the rain attenuation is more underestimated. The maximum values reached $A_{rain,max} = 0.69\ dB$ at 19.7 GHz and $A_{rain,max} = 3.6\ dB$ at 39.4 GHz whereas it should reach 25 dB at 19.7 GHz and more than 30 dB at 39.4 GHz. With the second method, the attenuation values are higher, $A_{rain,max} = 1.6\ dB$ at 19.7 GHz and $A_{rain,max} = 6.9\ dB$ at 39.4 GHz. The CCDF curve matched pretty well the one obtained from real measurements for low attenuation values (0-5 dB), but for higher values, the attenuation performance is still way lower than the real measurements.

The gas attenuation CCDF seems to offer pretty good results compared to the real measurements CCDF at 19.7 GHz even though the computed values are slightly higher. At 39.4 GHz, the gap between the two CCDF increases, especially for the oxygen attenutation, which reached 0.7 dB instead of 0.5 dB.

Finally, the total attenuation was computed. The maximum values reached are $A_{total,max} = 3.5\ dB$ at 19.7 GHz and $A_{total,max} = 12.2\ dB$ at 39.4 GHz with the rain rate computed with the first method, and $A_{total,max} = 2.4\ dB$ at 19.7 GHz and $A_{total,max} = 8.1\ dB$ at 39.4 GHz with the rain rate computed with the second method. As expected the total attenuation values reached are quite low when comparing to the Alphasat measurements. Whereas the rain attenuation is supposed to be the highest type of attenuation, when using the ERA5 dataset, the rain attenuation is not high enough. This cause the total attenuation to be lower than expected.

To conclude this work, it can be finally said that the ERA5 dataset can be used to estimate cloud and gaseous attenuation if the prediction is not required to be extremely accurate. However, the rain attenuation is highly underestimated. Even though the ERA5 dataset has a better spatial resolution than the previous reanalysis ERA-Interim, the resolution is still not fine enough to capture the localized and sporadic events such as rain. In order to optimize the attenuation prediction, high resolution Numerical Weather Prediction models could be used, or alternatively, new methods to derive more realistic rain values should be devised.

REFERENCES

[1] Administration, N. A. (1976). *U.S. Standard Atmosphere.*

[2] Bahri, R., Yarmohammadi, H., Keshavarzi, M., & Moradi, G. (2015). Typical Ka band Satellite Beacon Receiver Design for Propagation Experimentation. *Journal of Advances in Computer Engineering and Technology*, 23-28.

[3] Bohren, C. F., & Huffman, D. R. (1998). *Absorption and Scattering of Light by Small Particles.* Wiley-vch.

[4] Castanet, L., & Lassudrie-Duchesne, P. (2008). Propagation des ondes radioélectriques à travers l'atmosphere. *Techniques de l'ingénieur Système radars*.

[5] Chaudhary, K., & Vishvakarma, B. (2009). Effect of Ionosphere Induced Depolarization on Satellite Solar Power Station. *Progress In Electromagnetics Research Letters*, Vol. 9, 39-47.

[6] Copernicus Climate Change Service (C3S) (2017): ERA5: Fifth generation of ECMWF atmospheric reanalyses of the global climate . Copernicus Climate Change Service Climate Data Store (CDS). (n.d.).

[7] Danielson, E. W., Levin, J., & Abrams, E. (2002). *Meteorology.* McGraw-Hill Higher Education.

[8] Doviak, J. D., & Zrnic, D. S. (1993). *Doppler Radar and Weather Observations.* San DIego: CA: Academic.

[9] *ERA5 - Forecast - Dataset*. (2020). Retrieved from https://www.ecmwf.int.

[10] Guifu Zhang, J., Vivekanandan, J., & Brandes, E. (2001). A Method for Estimating Rain Rate and Drop Size Distribution from Polarimetric Radar Measurements. *IEEE Transactions on Geoscience and Remote Sensing*, 830-841.

[11] Ippolito, L. (1989). *Propagation Effects Handbook for Satellite Systems Design: A Summary of Propagation Impairments on 10 to 100 GHz Satellite Links with Techniques for System Design.* National Aeronautics and Space Administration, Scientifc and Technical Information Division.

[12] ITU-R. (2005). *Recommendation ITU-R P.838-3, Specific Attenuation Model for Rain for Use in Prediction Methods.*

[13] ITU-R. (2019). *Recommendation ITU-R P.676-12, Attenuation by atmospheric gases and related effects.*

[14] ITU-R. (2019). *Recommendation ITU-R P.840-8, Attenuation due to clouds and fog.*

[15] Kinter, P. L., Humphreys, T., & Hinks, J. (2009). *GNSS and Ionospheric Scintillation.* InsideGNSS.

[16] Krupenie, P. H. (1972). The Spectrum of Molecular Oxygen. *Journal of Physical and Chemical Reference Data 1*.

[17] Marshall, J. S., & Palmer, W. M. (1948). The distriution of raindrops with size. *Shorter Contributions*, 165-166.

[18] McGraw-Hill. (2009). *Troposphere, Concise Encyclopedia of Science and Technology.*

[19] Quibus, L. (2020). *Modelling propagation impairments of Earth-Space link using Numerical Weather Prediction tools.*

[20] Rossi, T., & Al. (2016). Satellite Communication and Propagation Experiments Through the Alphasat Q/V Band Aldo Paraboni Technology Demonstration Payload. *IEEE A&E Systems Magazine*.

[21] Shieh, W., & Djordjevic, I. (2010). OFDM for Optical Communications.

[22] Srinivas, K. K., & Ramana, T. V. (2017). Severe Cause of Cloud Attenuation and Rain Attenuation on Space Communication Link at Milimetre Band and Differentiation betwen Rain Attenuation and Cloud Attenuation. *IEEE 7th International Advance Computing Conference.* Hyderabad, India: IEEE.

[23] Terry, P. (2013). *Top 10 Of Evrything.* Octopus Publishing Group.

[24] Ulbrich, C. W. (1983). Nautral Variations in the Analytical Form of the Raindrop Size Distribution. *Journal of Climate and Applied Meteorology*, 1764-1775.